J. Space Weather Space Clim. 2024, **14**, 10
© E. Richard et al., Published by EDP Sciences 2024
https://doi.org/10.1051/swsc/2024008

Available online at:
www.swsc-journal.org

Topical Issue - Space Climate: Long-term effects of solar variability on the Earth's environment

RESEARCH ARTICLE OPEN ACCESS

Advancements in solar spectral irradiance measurements by the TSIS-1 spectral irradiance monitor and its role for long-term data continuity

Erik Richard[1,*], Odele Coddington[1], Dave Harber[1], Michael Chambliss[1], Steven Penton[1], Keira Brooks[1], Luke Charbonneau[1], Courtney Peck[1], Stéphane Béland[1], Peter Pilewskie[1,2], and Tom Woods[1]

[1] Laboratory for Atmospheric and Space Physics (LASP), University of Colorado, Boulder, CO 80309, USA
[2] Department for Atmospheric and Oceanic Sciences, University of Colorado, Boulder, CO 80309, USA

Received 29 August 2023 / Accepted 19 March 2024

Abstract – The first implementation of NASA's *Total and Spectral Solar Irradiance Sensor* (TSIS-1) launched on December 15th, 2017, and was integrated into the International Space Station (ISS) to measure both the total solar irradiance (TSI) and the solar spectral irradiance (SSI). The direct measurement of the SSI is made by the LASP Spectral Irradiance Monitor (SIM) and provides data essential to interpreting how the Earth system responds to solar spectral variability. Extensive advances in TSIS-1 SIM instrument design and new *SI*-traceable spectral irradiance calibration techniques have resulted in improved absolute accuracy with uncertainties of less than 0.5% over the continuous 200–2400 nm spectral range. Furthermore, improvements in the long-term spectral stability corrections provide lower trend uncertainties in SSI variability measurements. Here we present the early results of the TSIS-1 SIM measurements covering the first 5 years of operations. This time period includes the descending phase of solar cycle 24, the last solar minimum, and the ascending phase of solar cycle 25. The TSIS-1 SIM SSI results are compared to previous measurements both in the absolute scale of the solar spectrum and the time dependence of the SSI variability. The TSIS-1 SIM SSI spectrum shows lower IR irradiance (up to 6% at 2400 nm) and small visible increases (~0.5%) from some previous reference solar spectra. Finally, initial comparisons are made to current NRLSSI2 and SATIRE-S SSI model results and offer opportunities to validate model details both for short-term (solar rotation) spectral variability and, for the first time, the longer-term (near half solar cycle) spectral variability across the solar spectrum from the UV to the IR.

Keywords: Spectral irradiance / Solar variability / Solar spectrum / Solar cycle

1 Introduction

The Sun is the dominant source of energy for the Earth's climate system (Kren et al., 2017) yet the full influence of solar variability on climate remains quantitatively incomplete. Solar forcing influences combined with other natural variabilities are complex in both magnitude and phase. Decoupling these natural influences from anthropogenic impacts is critical to understanding human attribution to the rate of change of Earth's surface temperature (Lean, 2017; Eyring et al., 2021; IPCC, 2023). While historically the measurements of the total solar irradiance (TSI) have provided the solar variability constraint (Tett et al., 2002; Meehl et al., 2003), the long-term measurements of solar spectral irradiance (SSI) are recognized as being increasingly important to fully elucidate the Sun-climate connection (Haigh, 2007, Gray et al., 2010; Ermolli et al., 2013; Solanki et al., 2013; Seppälä et al., 2014). The wavelength and height dependence of solar radiation deposition, including ozone absorption in the stratosphere, absorption in the ocean mixed layer, and water vapor absorption in the lower troposphere, all contribute to the "top-down" (Haigh, 1996; Kodera & Kuroda, 2002; Matthes et al., 2006; Wang et al., 2019) and "bottom-up" (van Loon et al., 2007; Meehl et al., 2008) mechanisms that have been proposed as possible amplifiers of solar forcing for ultraviolet (UV) and visible-infrared (Vis-IR) SSI variability, respectively. Therefore, the observational continuity of both the TSI and SSI are critical for advancing the understanding of the Earth's energy budget and the full impact of solar variability on influencing atmospheric photochemistry and climate (Hansen et al., 2005; Stephens et al., 2012;

[*]Corresponding author: erik.richard@lasp.colorado.edu

L'Ecuyer et al., 2015; Wild et al., 2013, 2015, 2019). Increasingly sophisticated coupled chemistry-climate model (CCM) simulations require as input not only TSI at the top of the atmosphere (TOA) (Eyring et al., 2021) but SSI variations at TOA as well (Hood et al., 2015; Matthes et al., 2017; Shindell et al., 2020). To this end, accurate and long-term SSI measurements are vital direct inputs for advancing scientific understanding of the wavelength-specific processes influencing atmospheric response and climate variability.

Central to elucidating the roles and connections of the Earth's radiative, chemical, and dynamical responses to solar influences are both the data quality and measurement continuity of solar irradiance records – without sufficient mission overlap, there will be little chance of tying records together with the necessary accuracy and trend stability to quantify true long-term climate signatures (Weatherhead et al., 2017). From over four decades of partial overlapping TSI measurements, it is now well established that irradiance variations correlate with the solar activity over the typical 10–13-year solar cycle and are on average ~0.1% higher at solar maximum than at solar minimum. However, the SSI varies considerably depending on the wavelength, typically larger relative variability in the UV and progressively less in the longer wavelengths of the visible through IR. Because of the relatively large UV variability over the solar cycle (~10% in the FUV: 115–200 nm and part of the MUV: 200–300 nm) early SSI measurement missions focused more on the shorter solar wavelengths to establish the strong correlations with the solar cycle. Consequently, it has been established that ultraviolet irradiance variations – that influence the middle and upper atmosphere – have significant impacts on the radiative heating and the ozone budget in the stratosphere (Haigh et al., 2010; Swartz et al., 2012; Ball et al., 2019).

Beginning with the *Solar Radiation and Climate Experiment* (SORCE), the effort was to establish a long-term data record for nearly the full solar spectrum (SORCE SSI measurements covered a continuous wavelength range of 115–2400 nm – an integrated region >96% of the TSI). The majority of this wavelength range was measured by the SORCE SIM instrument to provide the daily solar spectrum from 200 to 2400 nm for the long-term solar data record (Harder et al., 2005a). The SORCE mission operated for a full 17 years – long enough to provide for 2 years of overlapping measurements with the follow-on first *Total and Spectral Solar Irradiance Sensor* (TSIS-1) mission.

A key objective of the TSIS-1 mission is to extend the solar irradiance data records of TSI and SSI variability from the SORCE mission with improved versions of the Total Irradiance Monitor (TIM) and Spectral Irradiance Monitor (SIM) instruments. As shown in Figure 1, the TSIS-1 mission successfully overlapped with the SORCE mission for 2 years (2018–2020) during a period of solar minimum conditions and continued observations into solar cycle 25 (SC25). Several other LASP missions are also shown for reference in this timeline. These include the *TSI Calibration Transfer Experiment* (TCTE)[1], a TSI-only mission that launched a spare SORCE TIM instrument (Kopp & Lawrence, 2005) as a rapid response to mitigate a TSI gap after the *Glory* mission failed to reach orbit, and the *Compact Spectral Irradiance Monitor* – CSIM (Richard et al., 2019) and the *Compact Total Irradiance Monitor* – CTIM (Harber et al., 2019) flight demonstration (FD) missions that are both technology demonstrations for future SSI and TSI instrument concepts, respectively. Finally, for the future TSI and SSI measurements, the second *Total and Spectral Solar Irradiance Sensors* (TSIS-2) mission is currently in development to eventually be launched to partially overlap with the TSIS-1 mission in the 2025 (near solar maximum) time period.

Figure 2 illustrates the critical importance of having partially overlapping missions, focusing on the TSI measurements here, and the goal of the generation of a long-term, low-uncertainty composite solar record. For both the SORCE and TSIS-1 TIM instruments the measurement-to-measurement uncertainty (<10 ppm precision) is an order of magnitude smaller than the absolute uncertainty of the measurements. This means that a time series of coincident measurements from two instruments can be matched by scaling the measurements of the less accurate instrument (SORCE TIM) to agree best with the more accurate instrument (TSIS-1 TIM). Additionally, small trending differences during the overlap time period can provide validation of the independent long-term stability corrections applied, and ultimately reduce the combined uncertainty in the composite TSI record (Kopp, 2014, 2021). With respect to the SSI, the challenge of achieving a long-term composite is multidimensional in scope. Not only are temporal and spectral overlaps critical, but spectral resolution and sampling differences between sensors must be carefully understood. Thus, only through careful analysis of partial overlapping measurements can we begin to understand the long-term trends in solar spectral irradiance.

The following sections provide details of the TSIS-1 SIM SSI measurements for the first 5 years of operations. First, an overview is provided of the TSIS-1 SIM instrument and operations, including improvements in the absolute spectral irradiance calibration and new methodologies for long-term spectral degradation corrections. The results sections highlight both the absolute solar spectrum at the last solar minimum (late 2019) including comparisons to previous solar reference spectra and then present measurements of the solar spectral variability from the UV to the IR. The variability results are compared and contrasted to the previous SSI measurements (including partial overlapping observations with the SORCE SSI instruments during the end of SC24 and the last solar minimum). Finally, comparisons of the TSIS-1 SIM observations with both the NRLSSI2 and SATIRE-S SSI models are presented – from the short-term (solar rotational) variability to the long-term SSI changes during the ascending phase of SC25.

2 TSIS-1 SIM overview

The TSIS-1 SIM is a solar spectral irradiance radiometer designed to measure the SSI from 200 nm to 2400 nm in units of $\mathrm{W m^{-2}\ nm^{-1}}$. The SSI is defined as the solar spectral energy flux per unit area per unit wavelength normal to the solar vector at the top of the atmosphere (TOA) normalized to 1 AU. The instrument derives heritage from the SORCE SIM (Harder et al., 2005a,b) but has been redesigned based on lessons learned to improve absolute accuracy and lower uncertainties in spectral stability corrections (Richard et al., 2020). Like SORCE SIM, TSIS-1 SIM utilizes a Féry prism to disperse and image the solar radiation on a fixed focal plane. This is

[1] The TCTE TSI data products can be found at: http://lasp.colorado.edu/home/tcte/data/.

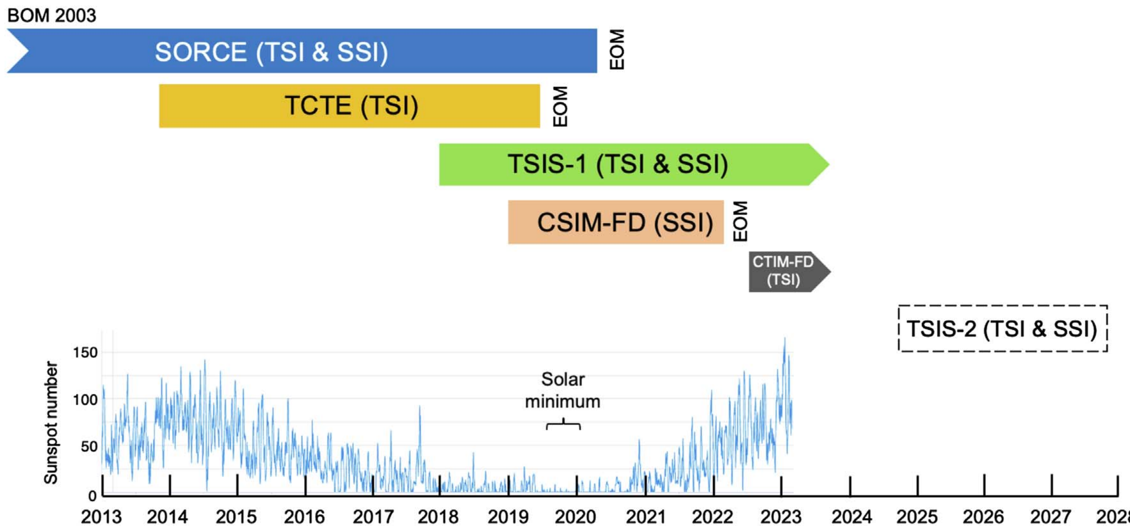

Figure 1. Timeline of LASP solar irradiance measurements over the prior and future decades. The SORCE mission launched in January of 2003 and was the first mission to contain a full solar irradiance suite, including a TSI instrument and several SSI instruments coving the X-rays through the near IR. Two new technology missions (CSIM-FD and CTIM-FD) overlapped with the TSIS-1 mission and provided direct comparison and validation of measurement performance. For the SSI, the CSIM-FD early mission and the TSIS-1 SIM observations overlapped during the time of the solar minimum conditions in late 2019 as shown by the lower plot of the sunspot number as a proxy for solar cycle activity for SC24 and the beginning of SC25.

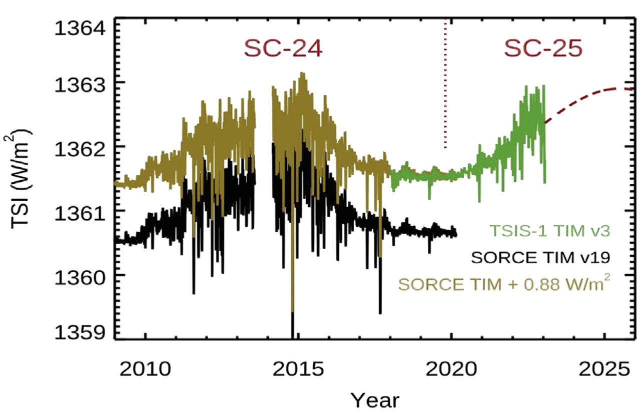

Figure 2. The TSIS-1 solar observations overlapped with SORCE measurements for two years during solar cycle minimum conditions. Shown here are the SORCE TIM and TSIS-1 TIM total solar irradiance measurements (SORCE TIM native TSI scale in black and then adjusted by 0.88 W/m^2 to match TSIS-1 TIM TSI scale at the TSI determined solar minimum time denoted by the dotted line). TSIS-1 measurements are now capturing the rise of SC25.

the only optical element within the instrument and provides spectral scanning through very precise prism rotation control using a closed-loop, optical-encoder mechanism (Harder et al., 2005a; Richard et al., 2019, 2020).

The TSIS-1 SIM incorporates improved detector performance in both the absolute electrical substitution radiometer (ESR) and the UV, visible, and near IR photodiode detectors. These detector improvements include higher signal-to-noise ratios and faster response times to those of the SORCE SIM. For the TSIS-1 SIM, we also completed a direct optical power calibration of the ESR. The SIM ESR is a bolometric detector that compares the heating effect of absorbed optical radiation with that of electrical power heating via an accurate, high-stability standard-Watt circuit. It is established as an *SI*-traceable calibration standard detector by pre-launch spectral calibrations against a cryogenic radiometer traceable to the US *National Institute for Standards and Technology* (NIST) Primary Optical Watt Radiometer (POWR), the principal US standard for radiant power measurements (Richard et al., 2020; White et al., 2022).

The ESR is the primary absolute detector and is used for two purposes: (1) the primary SSI measurement detector for the wavelength range 1650–2400 nm and (2) the long-term SSI calibration maintenance of the absolute radiant scale of the photodiode detectors that are used for daily rapid-scan, high signal-to-noise solar measurements over the range 200–1650 nm. The calibration maintenance approach involves using the Sun as the common calibration source to periodically calibrate the photodiode's radiant sensitivity response and track SIM channel-to-channel optical degradation changes. The TSIS-1 SIM optical layout and detailed descriptions for the SIM spectrometer design and pre-launch absolute calibrations have been discussed previously by Richard et al. (2020).

Another significant improvement for TSIS-1 SIM is having three redundant channels with one used frequently for daily spectrum cadence, one used for weekly spectrum cadence, and one used every 6 months for spectrum calibration maintenance. In contrast, SORCE SIM only had two channels, and long-term degradation tracking suffered from larger uncertainties in the stability corrections as cumulative solar exposure increased for both channels. To this end, redundant SSI measurement channels with differing observation cadences augment the ESR calibrations to provide more detailed instrument degradation corrections for improved spectral coverage and for more frequent calibration sampling.

For the long-term TSIS-1 SIM SSI observations, the SIM Channel A is used for twice-daily (~12-hour cadence) full spectrum observations. SIM Channel B observes a portion of the solar spectrum simultaneously with daily SIM Channel A on a ~weekly cadence for full spectrum coverage, and finally, SIM Channel C observes the full solar spectrum twice per year coincident with SIM Channel A and B observations. Comparisons of trends of the three channels have established that SIM degradation is primarily caused by cumulative solar exposure during the measurements. Optical degradation by space radiation (energetic particles) has been considered, but these effects appear to be minor as compared to direct solar exposure-time degradation. Therefore, the degradation rates for each SIM channel are derived using various exponential or linear decay functions as a function of cumulative solar exposure time (see Appendix A for details).

The TSIS-1 SIM data products include 12-hour and 24-hour averaged values and are operationally released for public use 5 days after acquisition (see Data availability statement). The TSIS-1 SIM is integrated into the International Space Station (ISS) and mounted on an independent solar tracking platform to provide precise (~1 arc-s, $1-\sigma$ uncertainty) solar pointing control to track the Sun during the sunlit portion of the ISS orbit. However, due to observational constraints related to ISS activities, there are times that SIM solar scans cannot be planned, these include periodic outages for visiting vehicle dockings and departures, astronaut EVA activities, and unfavorable ISS solar panel orientations – all activities that preclude normal solar scanning operations. The resulting SSI data gaps can be as short as a few hours and typically no longer than a couple of days. Seasonally, the ISS orbit encounters unfavorable solar beta angles that limit the amount of solar viewing time and also preclude complete solar scans. These periods, typically in May and December, last for approximately a week. For these periods, SIM solar scan sequences are modified to allow for the collection of at least one 24-hour (daily) SSI data product when favorable. As of 30 January 2023, 85% of the daily and 81% of the 12-hourly Level 3 data are available since the beginning of SIM operations on March 14, 2018.

3 Results

3.1 Solar spectrum comparisons

SORCE SIM and TSIS-1 SIM observations temporally and spectrally overlapped from March 2018 through February 2020 and provided an opportunity to compare the solar spectrum at solar minimum conditions between solar cycles 24 and 25. An example of the solar spectra comparison from TSIS-1 SIM and SORCE SIM is shown in Figure 3. The wavelength region covered by both instruments is 200–2400 nm. The spectra shown are plotted on their native irradiance scales and on a log-wavelength scale (to highlight the UV region of the spectrum). Both SIM instruments have the same spectral resolution due to the same dispersion geometries related to the fused silica Féry prism optical element. The inset in Figure 3 shows the ratio of the SSI spectra from TSIS-1 SIM to SORCE SIM for the majority of the spectrum – below 240 nm, the SORCE SIM instrument has large instrumental uncertainties due to lack of pre-flight calibrations and adverse scattered light effects. As can be seen here, there are spectral regions where there are significant differences in the SSI. The near UV region around 310 nm is at a detector transition region where the SORCE SIM is more sensitive to temperature effects. Furthermore, for the SORCE SIM, this region was shown to have relatively larger absolute uncertainties (>5%) based on FEL lamp pre-launch calibrations (Harder et al., 2010; cf. Fig. 2). The absolute calibration of the TSIS-1 SIM has been discussed in detail (Richard et al., 2020) and has been shown to have a pre-launch spectral irradiance calibration uncertainty of <0.5% based on direct tunable laser-based spectral irradiance calibrations against a NIST-traceable cryogenic radiometer. This low uncertainty was also validated in orbit by direct solar spectral measurements simultaneously with the CSIM-FD mission (Stephens et al., 2019). The CSIM SSI instrument was independently calibrated against the same NIST cryogenic radiometer and showed in-orbit agreement with TSIS-1 to <1% differences over the majority (250–2400 nm) of the measured spectrum (Richard et al., 2019; Stephens et al., 2019) – this level of agreement is within the combined standard uncertainties for both instruments.

The largest difference with respect to the integrated irradiance is in the near IR which shows a systematic decrease of TSIS-1 SIM SSI from the SORCE SIM SSI. This begins near 900 nm and continues to ~6% relative difference by 2400 nm. As noted in Harder et al. (2010), the SORCE SIM absolute scale in the 1300–2400 nm region showed up to 8% relative difference from the ATLAS3 reference spectrum (Thuillier et al., 2003) and was corrected to agree with ATLAS3 in this near IR wavelength range. A justification for this correction to the ATLAS3 irradiance scale for the near IR was a deficit in the SORCE SIM integrated spectral irradiance of ~30 $\mathrm{Wm^{-2}}$ that was not consistent with the 200–2400 nm integrated spectral irradiance value in comparison to the TSI value. Differences in the near IR SSI have been discussed previously regarding the solar spectra measured during the solar minimum conditions at the transition between solar cycles 23 and 24 (2008/09) (Thuillier et al., 2014). The comparisons presented include both measurements as well as two solar irradiance models. The overlapping measurements during this time period included the *Scanning Imaging Absorption Spectrometer for Atmospheric Chartography* – SCIAMACHY (Bovensmann et al., 1999) and the updated SOLar SPECtrometer (SOLSPEC) instrument on the second *Solar Monitoring Observatory* (SOLAR2) launched in February 2008 and integrated on the ISS (Thuillier et al., 2015). The models included the *Solar Radiation Physical Modelling* – SRPM (Fontenla et al., 1999, 2011) and the *Code for Spectral Irradiance* – COSI (Haberreiter et al., 2008; Shapiro et al., 2010). The results show that there are significant differences in the IR (outside reported individual instrumental calibration uncertainties) compared to the ATLAS3; the ATLAS3 irradiance between 1000 nm and 2400 nm is larger by 5–10%. The two physical models are consistent in showing relative near IR deficits from ATLAS3 of ~5% near 2000 nm and direct measurements of SCIAMACHY and SOLAR2 show larger relative deficits of ~10% near 2000 nm. Both SORCE SIM and the WHI reference (Woods et al., 2009) are consistent with ATLAS3, but as noted the SORCE SIM IR irradiance was adjusted to agree with ATLAS3, and the WHI composite

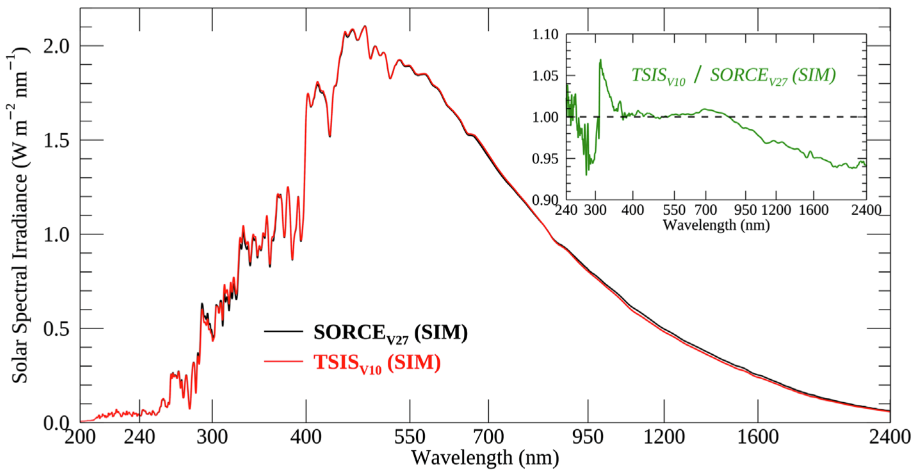

Figure 3. The SSI spectrum comparison of TSIS-1 SIM (red) and SORCE SIM (black) for the overlap time of TSIS-1 and SORCE missions covering the full range of 200–2400 nm (note: wavelength is plotted on a log-scale). Both spectra are plotted on their native irradiance scales (no scaling applied). The inset shows the ratio (green) as a function of wavelength over the 240–2400 nm range (below 240 nm, the SORCE SIM has large relative uncertainties). Clearly seen is the lower IR SSI longward of 900 nm, up to ~6% lower for TSIS-1 SIM. However, excellent agreement is seen throughout the visible where the SSI is a maximum.

Table 1. Integrated SSI compared to TSI for solar reference spectra. The common integrated region includes 205–2395 nm. ATLAS3 (Thuillier et al., 2003); WHI (Woods et al., 2009); SOLAR-ISS (Meftah et al., 2018).

Spectrum	205–2395 nm (W/m^2)	+52 (W/m^2)[b]	Adopted TSI value (W/m^2)	Diff from TSI (W/m^2)	Diff from TSI (%)
ATLAS3[a]	1333.6	1385.6	1361	+24.6	+1.8
WHI[a]	1321.0	1373	1361	+12.0	+0.9
SOLAR-ISS	1320.8	1372.8	1361	+11.8	+0.9
TSIS-1 SIM	1308.7	1360.7	1361.5[c]	−0.8	−0.06

[a] Excludes normalization to TSI.
[b] Common scalar offset accounting for unmeasured SSI <205 nm and >2390 nm.
[c] TSI measured same day as SIM first-light reference spectrum.

reference is based on the SORCE SIM spectrum for the IR wavelengths. The high accuracy measurement of the TSIS-1 SIM solar spectrum also shows a lower IR irradiance than ATLAS3 (and correspondingly SORCE SIM) by ~6% near 2400 nm, a systematic decrease between 1000 nm and 2400 nm that is consistent with both recent SCIAMACHY (Hilbig et al., 2018) and SOLAR2 (Meftah et al., 2020) re-calibrated solar reference spectra.

Table 1 summarizes the difference in the integrated SSI for various solar reference spectra (all representing near solar minimum conditions). The integrated region here encompasses 205–2395 nm. Note that for the ATLAS3 and WHI, the values exclude the *a-posteriori* normalization to the TSI in the final reported spectra. As can be seen, the ATLAS3 integrated value exceeds the TSI by nearly 2% (~25 Wm^{-2}) when accounting for the common irradiance outside the measured range. The spectral integral of the TSIS-1 SIM together with a common ~52 Wm^{-2} added to account for the missing irradiance outside of the measured region (Mauceri et al., 2018) yields a TSI value of only 600 ppm different than the actual TSI value measured by the TIM instrument during the same solar viewing time.

The TSIS-1 SIM measurements during the solar cycle minimum period near the end of 2019 have been used to develop a new, high-accuracy, solar reference spectrum called the *TSIS-1 Hybrid Solar Reference Spectrum* – HSRS (Coddington et al., 2021). The TSIS-1 HSRS is a composite reference spectrum that acquires its high accuracy between 200 nm and 2400 nm from the TSIS-1 SIM instrument (Richard et al., 2020) and from 2400 nm to ~2800 nm from the CSIM-FD CubeSat instrument (Richard et al., 2019). High spectral resolution, which is necessary for some Earth-science applications, is introduced by normalizing independent solar line data to the radiometric scale of the TSIS-1 SIM and CSIM instruments (Coddington et al., 2021 and references therein). In March 2022, the Working Group on Calibration and Validation (WGCV) of the Committee for Earth Observation Satellites (CEOS) endorsed the TSIS-1 HSRS as a solar irradiance reference spectrum standard (see Data availability statement).

Recently, the TSIS-1 HSRS has been extended down into the far ultraviolet (FUV) range of 115 nm and up into the far infrared (FIR) to 200,000 nm. This was completed to support additional Earth-science applications, such as detailed radiative transfer modeling, climate modeling, and SSI modeling. This new reference spectrum is known as the *Full Spectrum – Hybrid Solar Reference Spectrum* – FS-HSRS (Coddington et al., 2023). This wavelength extension required incorporating

Table 2. An integrated band comparison of the TSIS-1 SIM with both the FS-HSRS and the current solar forcing reference spectrum provided by the Coupled Model Intercomparison Project-Phase 6 (CMIP6), a dataset utilized in many current climate models.

Band	Band range (nm)	TSIS-1 SIM (W/m^2)	FS-HSRS (W/m^2)	CMIP6 (W/m^2)	$\Delta_{TSIS\text{-}1\ -\ CMIP6}$ (W/m^2) [%]	$\Delta_{FS\text{-}HSRS\ -\ CMIP6}$ (W/m^2) [%]
1	200–260	2.6855	2.6738	2.5422	0.1433 [5.637]	0.1316 [5.177]
2	260–340	42.2457	42.2241	41.8127	0.4330 [1.036]	0.4114 [0.984]
3	340–440	131.9235	131.9218	129.3265	2.5970 [2.008]	2.5953 [2.007]
4	440–630	359.3186	359.6758	356.0259	3.2927 [0.925]	3.6499 [1.025]
5	630–780	210.5653	211.2113	210.9445	−0.3793 [−0.180]	0.2668 [0.126]
6	780–1240	340.4387	340.9444	343.1782	−2.7395 [−0.798]	−2.2338 [−0.651]
7	1240–1300	25.5719	25.5966	26.0287	−0.4568 [−1.755]	−0.4321 [−1.660]
8	1300–1630	102.1468	102.2366	103.9975	−1.8507 [−1.780]	−1.7609 [−1.693]
9	1630–1940	53.5159	53.5694	54.7487	−1.2328 [−2.252]	−1.1794 [−2.154]
10	1940–2150	22.3023	22.2891	22.5943	−0.2920 [−1.292]	−0.3052 [−1.351]
11	2150–2500	–	23.5531	23.7459	–	−0.1929 [−0.812]
12	2500–3080	–	20.2597	20.3185	–	−0.0587 [−0.289]
13	3080–3850	–	12.0093	11.9903	–	0.0190 [0.158]
14	3850–12,200	–	12.7663	12.7411	–	0.0252 [0.198]

theoretical knowledge where no direct observations currently exist. The original HSRS encompasses ~97% of the TSI, and the extended FS-HSRS now integrates to the full TSI value to within 0.1% of direct observations of TSI by the TSIS-1 TIM instrument; a subsequent wavelength-independent scaling was applied to the final data product so the integral of the FS-HSRS equates to TSIS-1 TSI for that time period. The FS-HSRS spectrum is representative of the same solar minimum conditions of the TSIS-1 SIM observational era between solar cycles 24 and 25 (December 1–7, 2019). The spectral integral of the FS-HSRS spectrum from 115 nm to 200,000 nm yields a TSI value of 1361.5 ± 5.9 Wm^{-2} (a difference of <0.1% that is within uncertainties).

Table 2 shows a comparison of 14 separate, integrated bands from the UV (200 nm) to the longwave IR (12,200 nm) between the FS-HSRS and the solar forcing specified in the sixth *Coupled Model Intercomparison Project* – CMIP6 (Matthes et al., 2017), which is used in the solar forcing inputs to climate model runs in the IPCC Sixth Assessment Report (Eyring et al., 2021). Also shown in the table are the corresponding 10 bands observed by the TSIS-1 SIM that overlap with both the FS-HSRS and the CMIP6 spectrum. The TSIS-1 SIM Data Version 10 (V.10) values are taken from the same December 1–7, 2019 time frame as the FS-HSRS (see Data availability statement for data release notes). The values for CMIP6 solar forcing, which is specified by the average of the NRLSSI2 (Coddington et al., 2016) and SATIRE-S (Yeo et al., 2014) SSI variability models, are obtained from the previous solar minimum from November 21, 2008 to April 30, 2009.

These differences between both the FS-HSRS results and the TSIS-1 SIM observations from the CMIP6 spectrum for the common spectral bins are noted in Table 2 and are plotted in Figure 4. The FS-HSRS, by design, closely matches the integrated TSIS-1 SIM values in the 10 common bands. The irradiance scale of the CMIP6 spectrum is baselined from older and less accurate solar irradiance measurements and/or theory and the CMIP6 values are shown to differ more substantially from TSIS-1 SIM (and FS-HSRS). Both the TSIS-1 SIM and the FS-HSRS show enhanced visible irradiance and reduced infrared irradiance relative to the CMIP6 values. In the longest wavelength infrared portion, a region that is not directly measured by the TSIS-1 SIM, the FS-HSRS is consistent with a theoretical understanding of the magnitude of the solar spectrum (see Coddington et al., 2023 for details).

3.2 SSI variability observations

The direct measurements of SSI provide the spectral decomposition of the TSI, and together both observations are critical for a detailed understanding of the spectral variability of the solar irradiance. As discussed previously, the magnitude of the SSI variability varies considerably over a solar cycle, with shorter wavelengths (<400 nm) showing the largest relative variability – contributing nearly half of the TSI variability while only representing <7% of the TSI (Lean et al., 1997; Krivova et al., 2006; Woods et al., 2015). For the visible wavelengths, the relative variability is comparable to the TSI variability (~0.1% over the solar cycle) with progressively less variability for the longer IR wavelengths (predicted <100 ppm over the solar cycle) (Lean et al., 2005; Harder et al., 2009).

3.2.1 Ultraviolet variability

As noted previously, the long-term SSI observations have concentrated in the ultraviolet (and shorter wavelengths) due to the large relative variability and the strong impact on the upper/middle atmosphere, e.g. ozone photochemistry and radiative heating (Rottman et al., 2001; Woods, 2008). The SORCE mission provided the first continuous measurements of SSI covering a nearly full spectrum (115–2400 nm). In particular, the SORCE SIM instrument provided key new SSI observations of visible and near IR variability over the broad wavelength range of 200–2400 nm, an instrumental range that encompasses the spectral content of >96% of the TSI. However, the nearly 2-decade observational record of the SORCE SIM instrument was not without controversies. Perhaps most notable was the SORCE SIM measured SSI variability during the declining phase of solar cycle 23 from 2004 to 2009. The SORCE SIM UV irradiance variability showed ~3 times larger variability than previous measurements and model predictions. For example, in the integrated 250–300 nm region, representing ~13 Wm^{-2} (or ~1% of the TSI), SORCE SIM observations

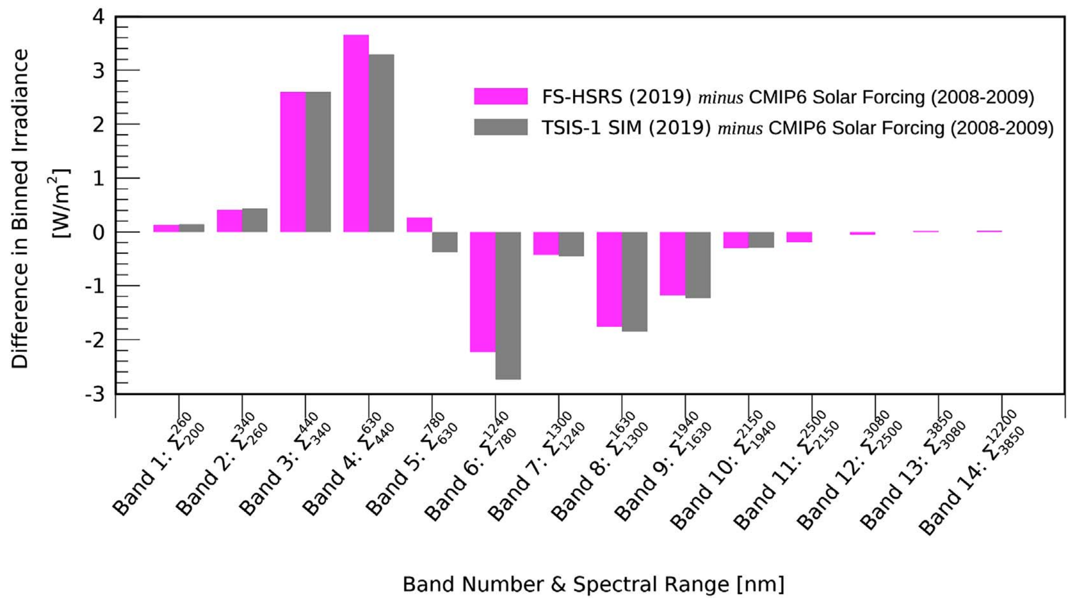

Figure 4. Binned spectral irradiance bands for both the FS-HSRS and TSIS-1 SIM compared against the CMIP6 solar forcing reference. The TSIS-1 SIM range cuts off at 2400 nm and therefore only covers bands 1 through 10. The integral of FS-HSRS(NRL4) from Band 1 through Band 14 = 1360.9312 Wm^{-2}; the Integral of the CMIP6 (avg from November 21, 2008 to April 30, 2009) from Band 1 through Band 14 = 1359.9950 Wm^{-2}; the integral of TSIS-1 SIM (V10 average spectrum covering December 1–7, 2019) from 200 to 2400 nm = 1309.42 Wm^{-2}.

showed a decrease from 2004 to the 2008/09 solar minimum of ~0.35 Wm^{-2} (>2.5%), where previous measurements (covering solar cycles 21–23) showed much smaller decreases (0.1 Wm^{-2}, or <1%) (Harder et al., 2009; Lean & DeLand, 2012). Such large SSI differences were at odds with upper atmospheric heating rates and ozone production and had significant impacts on the influence of solar variability on the stratospheric response in several model results (Haigh et al., 2010; Ball et al., 2011; Swartz et al., 2012). This caused much debate in the scientific community about the veracity of the SORCE SIM UV observations.

Given the consistency of the short-term (solar rotational) SORCE SIM variability with other measurements and models in the UV, questions about possibly larger-than-expected uncertainties in the long-term instrumental degradation corrections (that were unaccounted for in the published data) were considered. Figure 5 shows the SORCE SIM and SORCE SOLSTICE (McClintock et al., 2005a,b) and TSIS-1 SIM data records, plotted on their own irradiance scales, for the UV integrated irradiance in the 240–260 nm range – a spectral range that covers the O_3 Hartley absorption band). Evident here is the anomalously large irradiance variability of SORCE SIM for the declining phase of SC23 – over a factor of 3 larger than the SOLSTICE results. Also noticeable in the SORCE data is the significant decreasing trend through the 2008/09 solar minimum, inconsistent with other direct observations and historical proxies and indicative of under-corrected instrument degradation effects. For SC24 the agreement between the SORCE SSI instruments is better both in trending and magnitude of the solar variability. This is most likely a result of decreases in the optical degradation rates from the early mission operations.

The TSIS-1 SIM overlapped with SORCE instruments in the 2018–2020 time period (across the December 2019 solar minimum). For this period, both SORCE instruments show larger than-expected decreasing trends compared to the TSIS-1 SIM approaching solar minimum. For this 2-year overlap period in the 240–260 nm region, the UV integrated irradiance variability to solar minimum for SORCE SOLSTICE is ~0.4%, for SORCE SIM is ~0.2%, and the TSIS-1 SIM is <0.08%. As shown in Appendix A, the TSIS-1 degradation correction uncertainty in this wavelength region is <0.04% per year, and the trending result is within the 2-year stability correction uncertainty. These differences suggest that both SORCE SIM and SOLSTICE may have some residual, uncorrected degradation for this time period.

Figure 6 shows the UV SSI of several wavelengths for 5 years of continuous TSIS-1 SIM measurements. The time range includes March 2018 through January 2023, covering the last activity features in the decline of SC24, the solar minimum in late 2019/early 2020, and the ascending activity phase of SC25. Predictions place the next solar maximum in the late 2024 time period (Upton & Hathaway, 2023) indicating that SC25 is currently over halfway into its ascending phase. The plot shows the SSI covering 202 nm, 220 nm, 251 nm, and 280 nm. The active regions peak around 7–8% relative variability for the 202 nm (shortward of the 208 nm Al ionization edge) and 280 nm (core of Mg II line) with the corresponding 220 nm and 251 nm variability peaking near 3.5% for SC25 activity in January 2023. These values are consistent with the relative variability observed near the halfway point in the decline of SC24 (Woods et al., 2018). As discussed in Appendix A, these UV wavelengths show the largest instrumental degradation. For example, at 220 nm the spectral degradation is the largest and currently over 10% in channel A and 3.5% in channel B after five years of operations; recall that channel A (daily measurement channel) experiences the largest solar

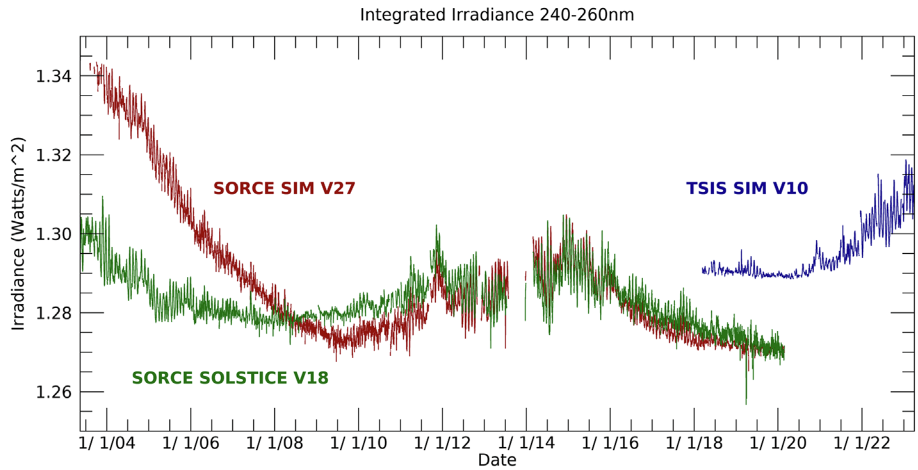

Figure 5. Comparison of solar UV irradiance in the 240–260 nm integrated region. SORCE covers 17 years of operations that overlapped for 2 years with the new TSIS-1 SIM measurements. The time period covers the decline of SC23, the full SC24, and the ascending phase of SC 25. Clear large differences in the UV variability in SC23 are obvious for the comparative measurements of SORCE SSI instruments. While SOLSTICE shows a variability consistent with both proxy-based and model UV irradiance variability predictions, the SORCE SIM variability appears to have large uncertainties in the instrumental degradation corrections (consistent with being under-corrected here). The new TSIS-1 SIM measurements – with significant improvements in signal-to-noise performance and stability corrections – are showing the last activity features of SC24 and the beginning increases of SC25. The SSI values for all instruments are plotted on their native reported irradiance scales.

exposure with channel B exposure at 11.8% that of channel A. Based on the spectral degradation corrections, the stability correction uncertainties for these UV wavelengths range from ~150 ppm/year at 280 nm to ~400 ppm/year at 202 nm at the native SIM resolution and sampling. These instrumental trend uncertainties in the complete degradation corrections were based on multiple SIM channel irradiance ratios tied to the SIM channel C calibrations (least exposed channel). Further evidence of the low uncertainties in the stability corrections is found in the lack of trending differences for all wavelengths across the solar minimum time period – consistent with all historical proxies for UV solar variability over many decades of solar observations (viz. Mg II index, Ly-alpha emission, F10.7 cm radio flux).

3.2.2 Visible/near IR variability

The SORCE SIM measurements of the long-term variability in the visible and near-IR (400–2400 nm) were not free of controversy either, especially for the declining phase of SC23. Relatively large variability, and in some cases out-phase behavior, relative to the TSI, were counter to the results of many proxy-based coupled-climate model simulations for visible and near IR solar variability inputs and showed anomalous heating rates inconsistent with known amplification mechanisms (van Loon et al., 2007; Meehl et al., 2008). For example, over the same time period (2004–2009) coincident with the large 0.35 Wm^{-2} decrease in 250–300 nm integrated UV irradiance, SORCE SIM showed a corresponding 0.3 Wm^{-2} (~0.2%) increase in visible energy at 600–700 nm – variability that was out-of-phase with TSI and controversial (Lean & DeLand, 2012). It should be noted that the measurement requirements to provide long-term SSI variability to detect solar trends at <0.1% over a decade are challenging, especially for an instrument that covers a large spectral range encompassing >96% of the TSI. For example, Figure 7 shows the 17-year SORCE SIM SSI in the integrated 500–600 nm visible region of the solar spectrum. Here there are clear irradiance signatures of solar activity (e.g. sunspot decreases and facular enhancements) corresponding to the declining phase of SC23 and the full SC24, however the out-of-phase behavior with TSI for the declining cycle SC23 is clearly evident. Taken together with the larger UV variability observed during this early mission time period leads to concerns about inadequately separating instrumental trending corrections from true solar variability. Like the UV data of Figure 6, the overall visible variability of SORCE SIM for SC24 appears to have less significant instrumental trending when compared to expectations based on historical solar cycle proxies. For the full SC24 from the 2008/09 minimum to the 2019/20 minimum, there is a long-term trending increase of ~0.015% (150 ppm) per year evident in the SORCE SIM results. For comparison, we show the TSIS-1 SIM 500–600 nm integrated data for the ascending phase of SC25 that is entirely consistent (both in-phase and relative change) with the TSI variability (cf. Fig. 2).

A reanalysis of the SORCE SIM data record from 2004 to 2012 using the concurrent measured TSI to constrain the integrated SIM uncorrected SSI along with the measured spectral dependence of the degradation function provided a revision of the SORCE SIM SSI variability (Mauceri et al., 2020b). The results of this study showed SIM UV variability for the declining phase of SC23 and the ascending phase of SC24 consistent with both the NRLSSI2 and SATIRE-S solar irradiance models within the expanded measurement uncertainties. Additional, independent analyses showed similar results to Mauceri et al. (2020b) attempting to separate true solar cycle irradiance variability from residual instrumental degradation trends across the solar spectrum: the Multiple Same Irradiance Level (MuSIL) technique using different times but common irradiance periods across multiple solar cycles to provide long-term trends in SSI

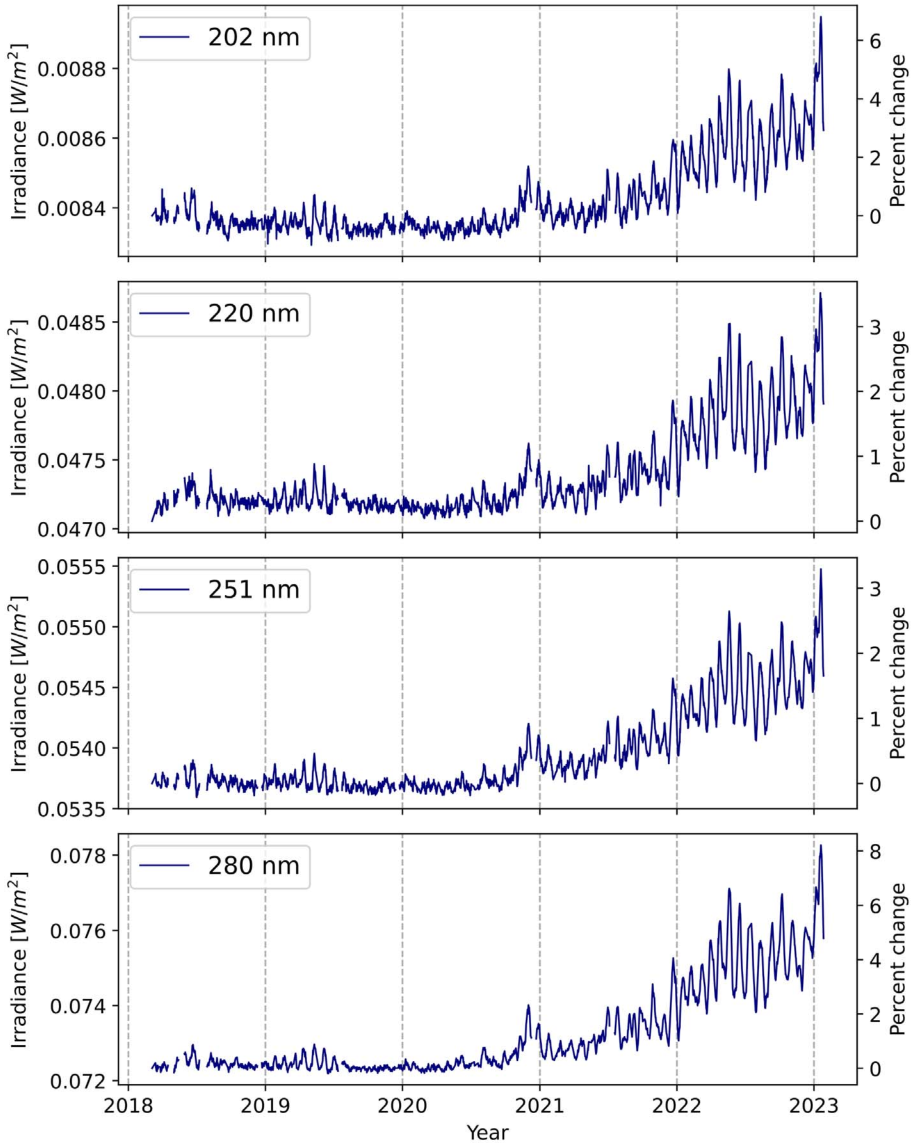

Figure 6. The TSIS-1 SIM Level 3 Version 10 (V.10) time series is shown at select wavelengths in the UV over the current mission. Left axis shows the absolute irradiance scale and the right axis shows the relative change (in %) from the first day of operations (March 14, 2018).

(Woods et al., 2018) and a mathematical framework study decoupling instrumental trends from solar irradiance data by comparing the observed variability with several solar proxies such as the F10.7 index, the MgII index, and the sunspot number (Dudok de Wit, 2022).

Figure 8 shows the same five years for the TSIS-1 SIM continuous measurements over several selected visible and near IR wavelengths: 471 nm, 652 nm, 857 nm, and 1035 nm. These are four representative wavelengths that were shown by Harder et al. (2009) to have alternating in-phase to out-of-phase long-term trending between SORCE SIM SSI and TSI. The relative variability here (referenced to the start of operations in mid-March 2018) is shown on the right axis for each wavelength, decreasing from ~0.15% at 471 nm down to <0.06% at 1035 nm. The channel-to-channel degradation corrections are applied here and result in stability correction uncertainties in the 20–50 ppm/year based on the standard deviations of the exponential fits for the correction factors over these wavelengths (see Appendix A).

Dark sunspot passage depletions and limb facular brightening in the irradiances are clearly observed at all these wavelengths with the onset and increasing activity in SC25. For the near IR wavelengths, a small, periodic irradiance variation correlating with a residual Earth-Sun distance (1 AU) differential effect is present at the ~100 ppm level (most noticeable in the early 2018–2021 range). These small artifacts are currently under further investigation but are believed to be caused by a combination of effects related to the sensitivity of the temperature correction coefficients of the Si- and InGaAs-photodiodes; the Si detector long wave cutoff is near 900 nm and the InGaAs detector shortwave cut off begins near 1000 nm. The radiant sensitivity values of these detectors have large response gradients (in Amps per Watt) in the cutoff regions and consequently, the temperature correction uncertainties increase. Additionally,

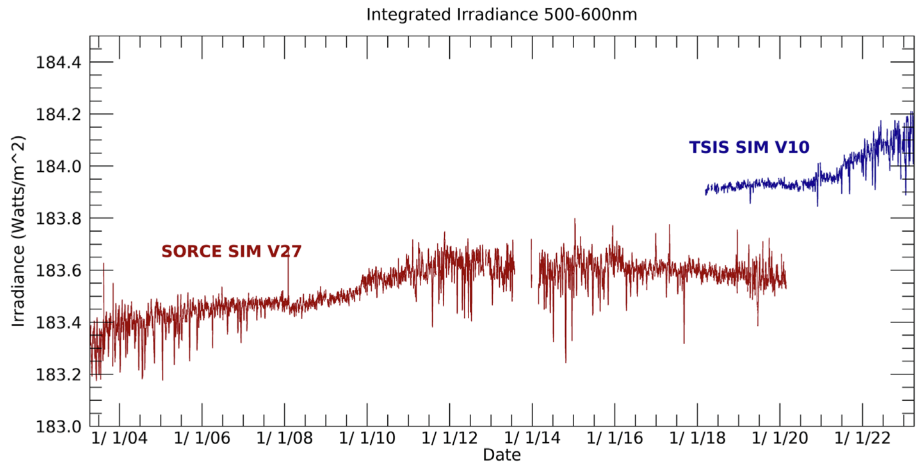

Figure 7. Comparison of solar visible irradiance in the 500–600 nm integrated region for the SORCE SIM and the TSIS-1 SIM. Again, the time period covers the decline of SC23, the full SC 24, and the ascending phase of SC25. Integrated irradiances are plotted on the native scales of each instrument. Notice for the SORCE SIM, the irradiance for the declining phase of SC23 (2004–2008) shows a trend out-of-phase with the TSI, however for SC24 there appears to be an in-phase relationship from 2008/09 minimum to 2019/20 minimum. Based on a linear trend covering the full SC24, SORCE SIM results here are consistent with ~150 ppm/year increase – a rate at the limit of the instrumental stability corrections. The TSIS-1 SIM irradiance from the last solar minimum into the ascending phase of SC25 is highly correlated with TSI (see text).

there are larger diffraction corrections (~4% maximum) applied in the measurement equation algorithms and a small residual error at the 100 ppm level is possible. Both adverse effects are currently being further evaluated and will be refined for future TSIS-1 SIM data versions (released approximately at 6-month intervals throughout the mission).

Another useful way to present the solar variability for the onset of SC25 is to correlate the relative spectral irradiance variability directly with that of the corresponding TSI variability. Figure 9 shows the correlation plots of the visible and near IR SSI variability relative to the TSI variability for the wavelengths shown in Figure 8. As can be seen, near linear correlations exist (and all in phase) with progressively decreasing SSI variability from shorter to longer wavelengths relative to TSI variability (i.e., ΔTSI/ΔSSI slope increases with increasing wavelength). These results are largely consistent with the results of spectral correlations of SSI and TSI with solar activity (Wehrli et al., 2013) measured by the *Variability of solar IRadiance and Gravity Oscillations* (VIRGO) experiment (Fröhlich et al., 1995) on the *Solar and Heliospheric Observatory* (SOHO) satellite with over a decade of measurements spanning 2002–2012 – a time period covering the full descending phase of SC23 and the early activity of SC24. The three VIRGO Sun Photometer (SPM) spectral bands spanned the near UV to the near IR and were centered at 402 nm, 500 nm, and 862 nm. Based on monthly comparisons, positive correlations of SSI with TSI were reported at all three wavelengths, consistent with the TSIS-1 SSI and TSI correlations shown here. For example, at 500 nm, the VIRGO SPM ΔTSI/ΔSSI correlation (slope) was reported as +0.61. This value is in very good agreement with the TSIS-1 SIM 500 nm correlation of +0.66 ± 0.004. The near agreement of this mid-visible SSI to TSI variability correlation from the decline of SC 23 and rise of SC24 with the recent rise of SC25 is consistent with the expectations of the visible SSI variations being completely in-phase with solar cycle variability (Haberreiter et al., 2017).

Close examination of the correlation plots for the shorter wavelengths (e.g. 470 nm and 652 nm) shows a possibility of bi-linear behavior; the correlation slopes appear slightly different during the early mission (solar minimum time frame) compared to the later two years (rise of SC25). This is currently under further investigation with respect to either potential refinements in the degradation rate corrections based on increasing irradiance in the damaging UV wavelengths or possibly due to true solar variability changes between the SSI and the TSI evolving during the solar cycle.

3.2.3 Integrated SSI variability

A condition on the SSI is that the integral over all wavelengths must equal the TSI. The TSIS-1 SIM instrument measures the solar spectrum from 200 nm to 2400 nm, an integrated region that makes up 96.2% of the TSI. The difference is 3.8% (~52 Wm^{-2}) of solar irradiance <200 nm and >2400 nm (wavelengths not directly measured by TSIS-1 SIM) with the overall majority of this irradiance deficit due to the IR SSI longward of 2400 nm. This long wavelength region of the spectrum is predicted to show very small relative variability where studies have shown that the solar cycle variability of this ~52 Wm^{-2} irradiance longward of the 2400 nm SIM cutoff is $\leq$0.02% (Yeo et al., 2014; Mauceri et al., 2020b).

Figure 10 shows the 5-year continuous record of the comparison of the measured TSI by the TSIS-1 Total Irradiance Monitor (TIM) and the spectrally integrated SSI from the TSIS-1 SIM plus a constant 52.13 Wm^{-2} offset. The comparison shows excellent long-term trending agreement within a $1 - \sigma$ standard deviation of ~50 ppm (0.068 Wm^{-2}) over the first 5 years of observations. However, there are time periods during the mission where there are larger, localized differences observed. These time periods include the beginning of the mission (March–April 2018) where SIM degradation corrections have larger relative uncertainties as well as June–July 2020

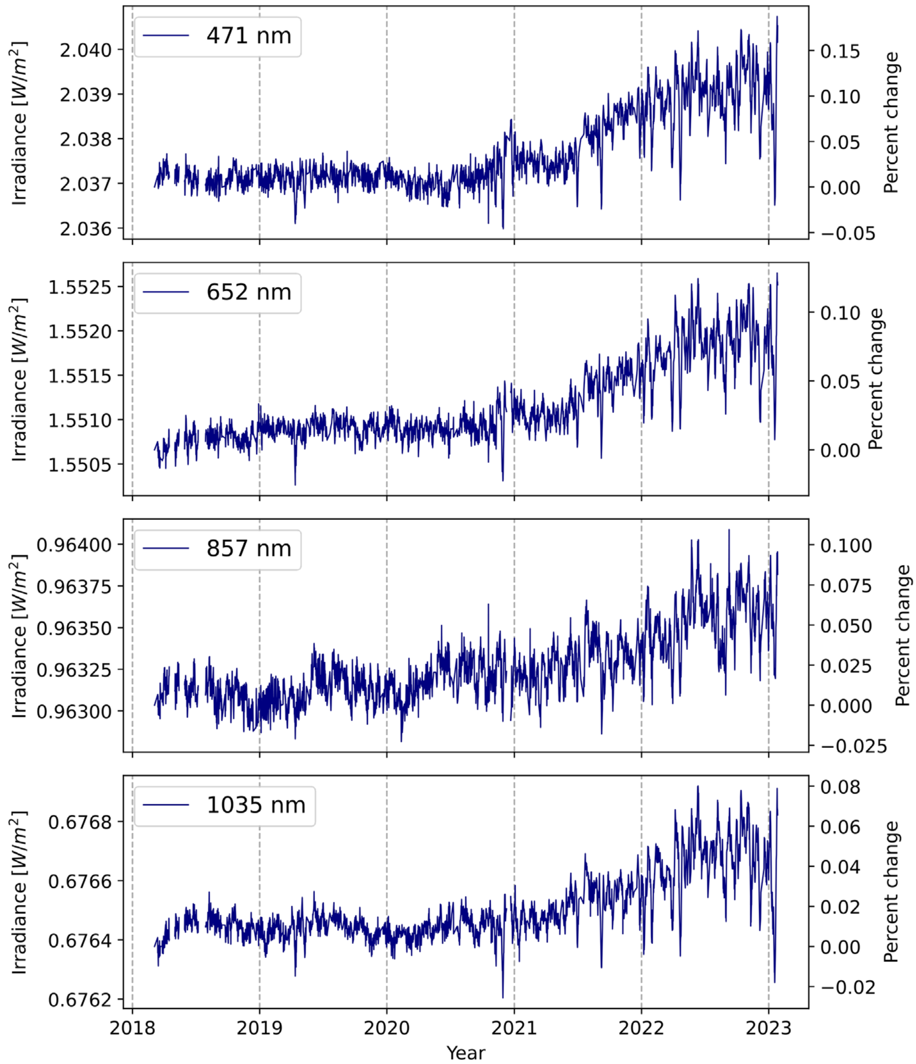

Figure 8. The TSIS-1 SIM (V10) time series is shown at selected wavelengths in the visible and near IR, over the first 5 years of the mission. Left axis shows the absolute irradiance and the right axis shows the relative change (in %) from the first day of operations (March 14, 2018). Note the decrease in the relative variability in the ascending phase of SC25. Also, note that all wavelengths are in phase with the TSI, counter to the early findings of Harder et al. (2009) for previous cycles. The presence of a residual annual cycle in the longest wavelengths (at the 0.01% level) is instrumental in origin and discussed in the text.

where the SIM instrument experienced higher than nominal temperatures due to a temporary ISS orbital orientation change. Figure 10 also shows the high correlation of the integrated SIM SSI with the TSI to capture all the short-term solar activity irradiance changes. To highlight this, Figure 11 shows the expanded view of the comparison for the year from January 2022 to February 2023 where SC25 solar activity was increasing. All TSI variability is captured in the integrated SSI over the full dynamic range of irradiance changes due largely to sunspot and facular influences.

The agreement shown in Figure 10 provides validation of a necessary condition for the integrated SSI variability over the mission to date and gives confidence in the spectral degradation corrections for SIM (and TIM). It is important to note here that the SIM results are completely independent – the TSI data from TIM was not used in any way as a boundary condition or constraint in the final spectral degradation corrections for SIM. As discussed in detail in Appendix A, the TSIS-1 SIM degradation corrections are done entirely based on inter-channel spectral ratio comparisons involving differing solar exposure rates on the different SIM channels.

While it is true that immutable agreement of the integrated SSI with the TSI is a necessary condition, it is not a sufficient condition to fully validate the correctness of the relative magnitudes of the TSIS-1 SIM spectral correction factors. Indeed, an infinite number of individual spectral contributions can integrate into the same TSI value. However, based on the direct, low uncertainty measurement of the spectral degradation rates by the channel-to-channel SSI ratios between all three SIM channels, we have determined the known spectral degradation function across all wavelengths (Appendix A) and the methodology remains robust against added SIM channel C calibrations with mission time. The dominant irradiance in the visible and near IR wavelengths are the major contributions to the integrated

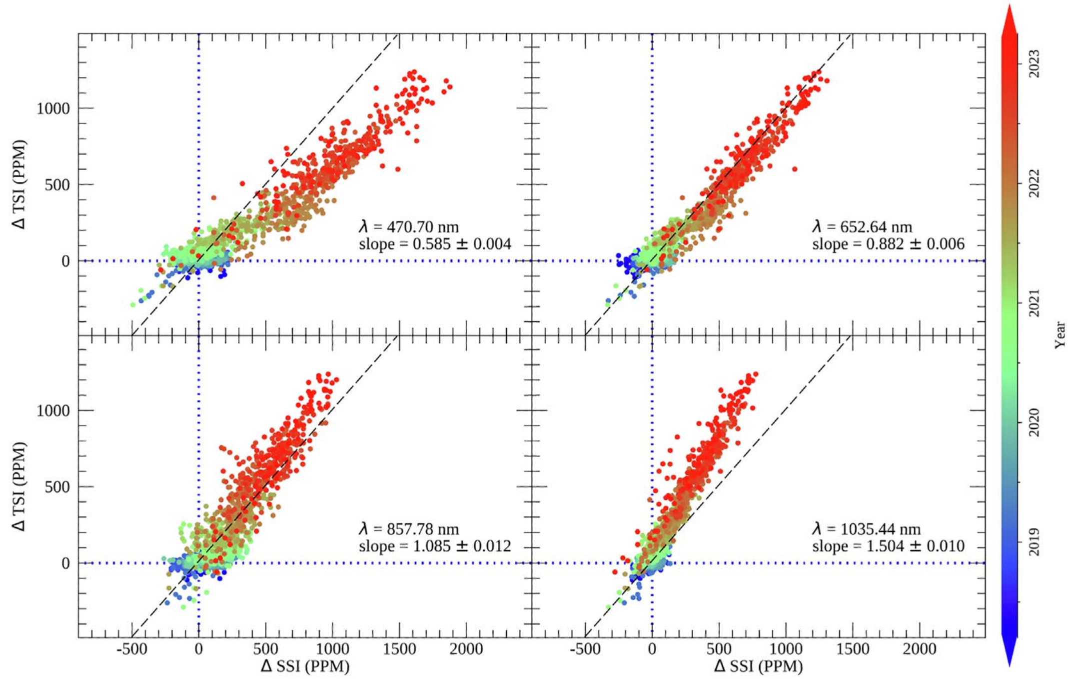

Figure 9. Correlations between TSIS-1 TIM TSI and SIM SSI variability during the ascending phase of SC25 for selected visible and near IR wavelengths: 471 nm, 653 nm, 858 nm, and 1035 nm. All cases show strong, positive (i.e., in-phase) correlations against the TSI. Blue dotted lines denote the solar minimum period in late 2019 and the black dashed lines represent the unity slope (1:1 variability). These results show that the SSI variability near 470 nm is ~70% greater than that of the TSI whereas at the longer wavelengths in the near IR (1035 nm), the SSI variability is ~30% less than the TSI variability.

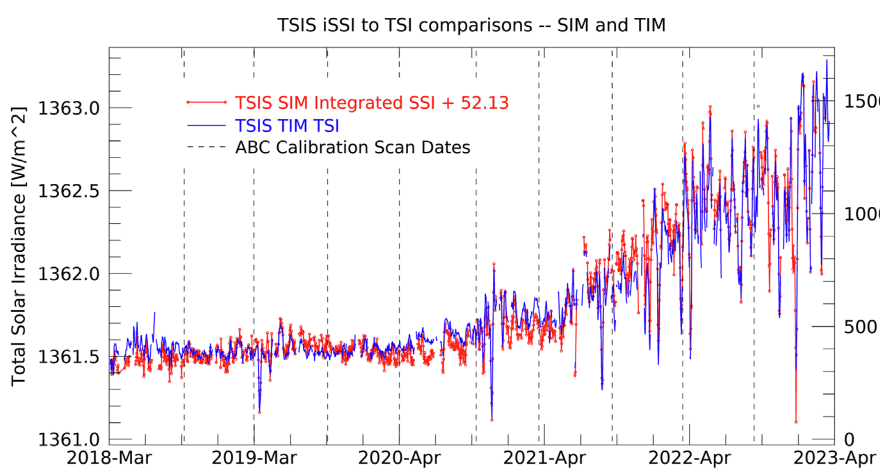

Figure 10. Comparison of the integrated (200–2400 nm) SIM SSI (iSSI: red) to the TSIS-1 TIM measured TSI (blue). A constant offset of 52.13 $\mathrm{Wm^{-2}}$ has been added to the integrated SIM to account for the irradiance outside of the SIM measurement range (mostly >2400 nm) to put it on the TIM TSI scale. The agreement with the TSI short-term variability and the long-term trending over the full mission is excellent with an overall difference from the TIM TSI of 0.068 $\mathrm{W/m^2}$ (<50 ppm, 1σ) over the first five years of continuous observations. The SIM Channel A, B, & C calibration dates noted are the 6-month cadence calibrations to constrain the spectral degradation functions to the SIM channel C observations (see Appendix A for details). New version releases occur after each of these calibrations to provide updates on the stability correction uncertainties by further refinements in the measured spectral degradation functions.

SSI and even small errors in the degradation corrections would be noticeable deviations in the TSI comparisons. The observed standard deviation of ~50 ppm difference over five years of operations offers strong support for the consistency of the spectral stability corrections over these wavelengths that dominate the solar energy distribution. However, errors in the magnitude of the UV degradation corrections may not be evident in the integrated comparison, largely because the UV irradiances contribute much less to the TSI. However, the larger magnitude of the spectral degradations for the UV wavelengths during the

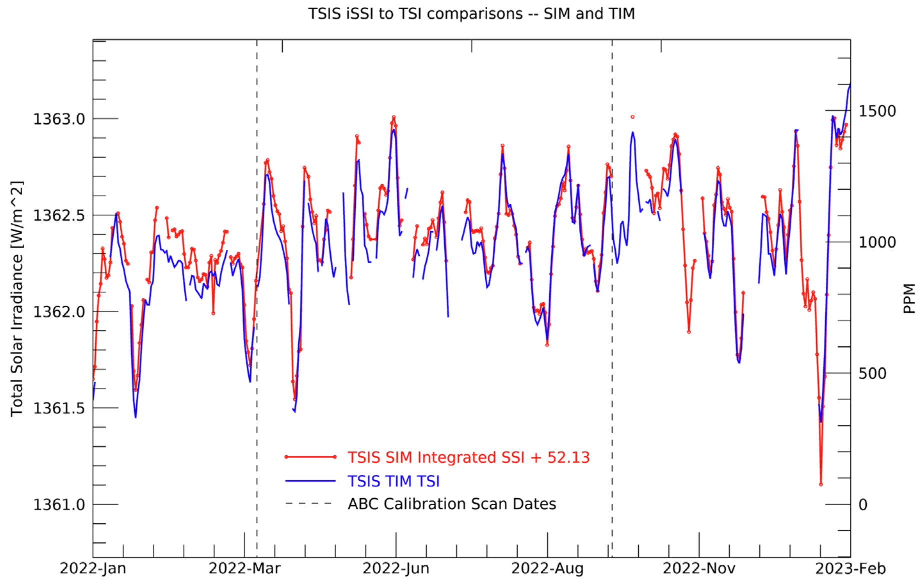

Figure 11. Comparison of the integrated (200–2400 nm) SIM (iSSI) + 52.13 Wm^{-2} (red) to the TSIS-1 TIM measured TSI (blue) covering the year 2022 (January 1, 2022–February 1, 2023). This shows the excellent agreement for both the annual trending as well as the short-term (solar rotational) structure during activity in SC25. Note that some differences are due to sampling differences in the interpolation of the measurements to a common temporal grid (due to the different timing of the daily observations). Small data gaps for each instrument are specific to ISS activities that preclude measurements and are different for each sensor.

solar minimum period allowed for strong exponential decay correlations to provide instrumental decay rates in the absence of solar activity.

4 Comparison with SSI models

4.1 NRLSSI2 and SATIRE-S SSI models

The more accurate SSI observations by TSIS-1 SIM are being used to extend the SSI climate record and to improve SSI models. Currently, the two models that provide comprehensive reconstructions of solar irradiance (both TSI and SSI) and are relevant to providing SSI variability inputs to the broader Sun-climate communities are version 2 of the Naval Research Laboratory Solar Spectral Irradiance – NRLSSI2 empirical model (Lean et al., 2005; Coddington et al., 2016) and the Spectral And Total Irradiance REconstruction for the Satellite era – SATIRE-S semi-empirical model (Krivova et al., 2003; Yeo et al., 2014). Both the TSI and SSI observational records established the primary contributions of dark sunspots and bright faculae in producing variability in the solar output (Willson et al., 1981; Chapman, 1987; Solanki & Unruh, 1998; Fligge et al., 2001; Lean et al., 2020). The dark sunspots deplete local solar emissions and reduce the disk-integrated irradiance in the visible and infrared spectral regions. Conversely, the bright faculae associated with active regions and more distributed active networks are longer lasting than the sunspots and consequently produce enhancements in the irradiance showing strong spectral dependence in the ultraviolet spectral regions. The two influences act in opposition as solar surface active regions form, evolve, and decay. The net result is a modulation of the relative strengths and phases of the sunspot and facular contributions to the solar irradiance variability. Both the NRLSSI2 and SATIRE-S solar irradiance models have been developed to utilize these sunspot and facular influences as well as surface magnetic features through magnetograms and continuum intensity images (Lean et al., 1998; Unruh et al., 1999; Krivova et al., 2003; Yeo et al., 2014). Ultimately, the disk-integrated solar irradiance from these SSI models is derived by integrating over the solar surface, accounting for the presence of these dark (sunspots) and bright (faculae and network) surface magnetic features.

To quantify the sunspot darkening and facular brightening contributions, information about active region size and distribution across the entire solar disk is obtained typically from solar images and magnetograms (Lean et al., 1998; Preminger et al., 2002; Krivova et al., 2003). Unlike the localized sunspots, the irradiance brightening enhancements are more widely dispersed with active area evolution across the entire solar disk. Empirical methods (e.g. NRLSSI2) using the Mg II chromospheric emissions have been developed to quantify the spectral dependence of the variability since photospheric faculae underlie the bright chromospheric plage of these active regions (Lean, 2000). Alternatively, the more physically based model approach to spectral irradiance reconstruction utilizes either full-disc magnetograms and intensity images (e.g., Yeo et al., 2015; Krivova et al., 2011) or Ca II K and red continuum images (e.g., Fontenla et al., 1999; Ermolli et al., 2011; Criscuoli et al., 2023) to define the fraction of the solar surface covered by the sunspots and faculae in conjunction with spectral intensities from semi-empirical model atmospheres (e.g., Fontenla et al., 1999; Unruh et al., 1999).

4.2 Short-term SSI variability

Active region onset, evolution, and decay during the current ascending phase of solar cycle 25 are used in an ongoing analysis of multiple rotational periods that yield the statistics of SSI

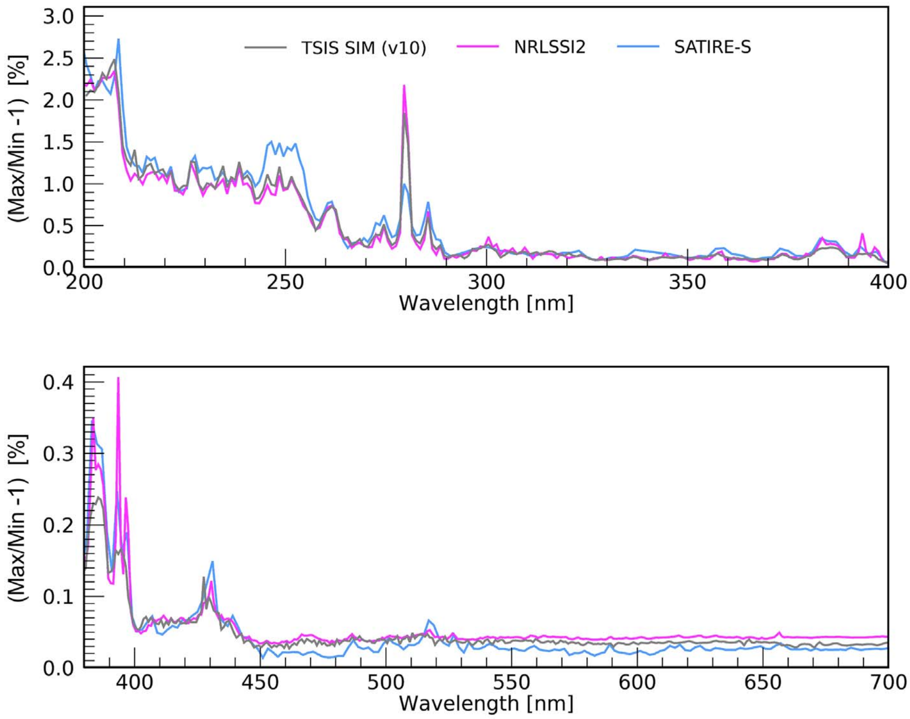

Figure 12. Comparison of the solar rotational relative spectral variability between TSIS-1 SIM observations (grey) with the NRLSSI2 model (pink) and SATIRE-S model (blue) for active region contrast in August 2022 when multiple active regions were present during a solar 27-day rotational period. Here maximum activity condition is the average SSI for the August 9–12, 2022 time frame, and the minimum activity condition is represented by the average SSI for August 23–26, 2022 (see Fig. 13).

short-term solar variability in the faculae and sunspot-dominated periods. The current NRLSSI2 model version utilizes a parameterization of the rotational irradiance variability from the SORCE era (SORCE SOLSTICE and SIM), with an additional correction to solar cycle TSI variability as observed by SORCE TIM that adds uncertainty. The TSIS-1 SIM SSI observations are being used to directly improve the NRLSSI2 model coefficients that scale solar magnetic variability to irradiance changes (Lean et al., 2022). This will directly benefit advancing the solar irradiance climate data record (CDR) algorithms that implement parameterizations based on solar rotational (~27 days) SSI variability that will be validated against the long-term solar cycle SSI observations (Coddington et al., 2016). These validation efforts compare the observed faculae and sunspot spectrally dependent contrast factors with those used in the model parameterizations. Figure 12 shows an expanded view of the active region contrast of solar rotational variability in August 2022 when multiple active regions were present on the solar disk early in SC25. To visualize the distribution of this activity, Figure 13 shows the NASA SDO HMI line-of-sight (LOS) synoptic activity map (for Carrington Rotations 2260 & 2261) during this August 2022 time period and highlights the "active" (maximum) and "quiet" (minimum) regions used in the SSI contrast comparisons shown in Figure 12.

With respect to the short-term SSI relative variability comparisons shown in Figure 12, the NRLSSI2 model (again, parameterized based on the SORCE-era rotational spectral contrasts) shows very consistent agreement with the TSIS-1 SIM observations, both in terms of fine-scale solar spectral variability structure as well as the amplitudes associated with the variability magnitudes. In contrast, the semi-empirical SATIRE-S model shows relatively larger UV irradiance variability most noticeable near wavelengths of the dominant emission line cores and Al- and Mg-continuum edges (Lean et al., 2022). Additionally, for this active region comparison, the SATIRE-S sunspot contrast factors produce lower visible irradiance variability showing nearly a factor of two decrease from the observations for some wavelength regions (particularly 460–480 nm and 550–610 nm). Building on the successful SSI CDR analysis (Coddington et al., 2016), the recent results suggest that improvements in the NRLSSI2 darkening contrast factors due to sunspots can be done that will reduce the overall uncertainties arising from assumptions in the current differential darkening parameterizations. The TSIS-1 SIM observations are being used in a new/improved model that will become version 3 of the NOAA/NCEI Solar Irradiance CDR in August 2024. As solar activity during the ascending phase of SC25 increases towards solar maximum, it is anticipated that the TSIS-1 SIM observations will provide valuable information to further refine both the NRLSS2 and SATIRE-S models over many rotational scale activity features.

4.3 Long-term SSI variability

The improved spectral stability performance of the TSIS-1 SIM over previous SSI instruments is allowing the opportunity, for the first time, to validate SSI models directly against longer, near solar cycle, timescales. Figures 14 and 15 show the comparison of the TSIS-1 SIM full (200–2400 nm) measurement record over the mission to date (March 2018–January 2023). These comparison plots cover several key band-integrated

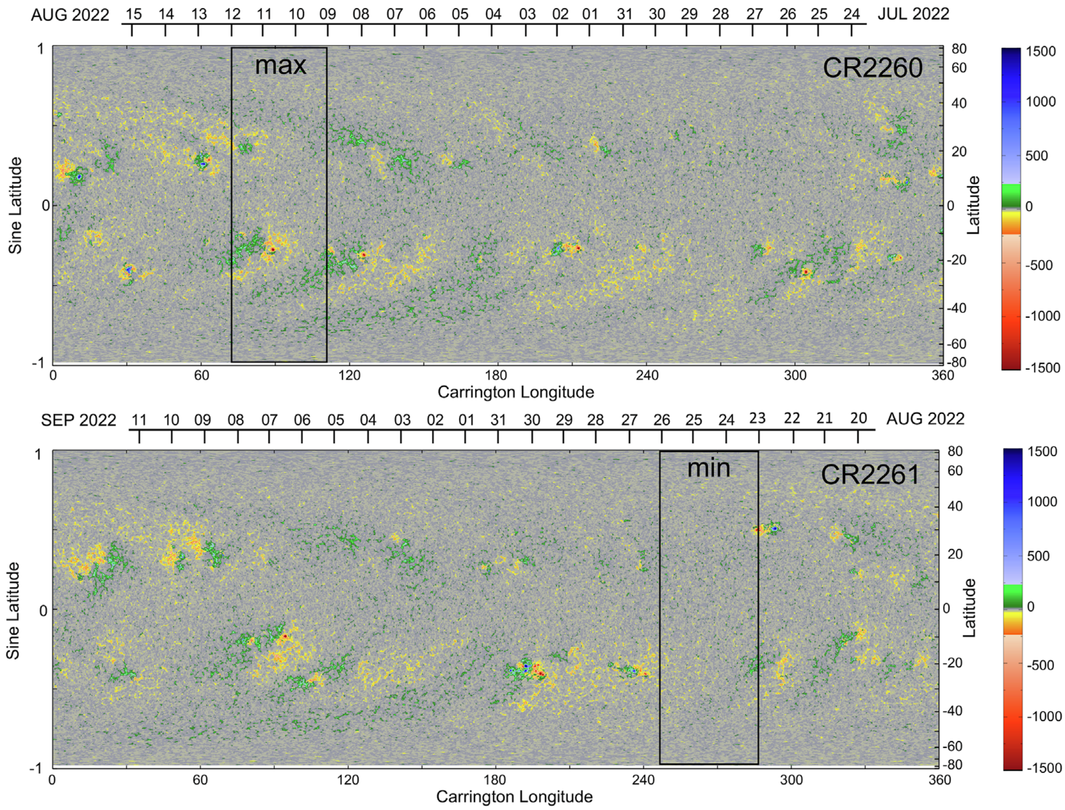

Figure 13. HMI line-of-sight (LOS) synoptic charts showing magnetogram images of solar activity for early and late August 2022 (covering CR2260 & CR2261) highlighting the time periods for the active region days used for the short-term irradiance variability shown in Figure 12. For the SSI variability plot in Figure 12, the maximum and minimum activity periods are defined as SSI averages over ~4 consecutive days for disk-centered times of August 9–12, 2022, and August 23–26, 2022, respectively. (Images courtesy of NASA/SDO and the HMI science team: http://hmi.stanford.edu/data/synoptic.html).

spectral regions from the UV to the shortwave IR: 265–285 nm (UV), 310–400 nm (NUV), 400–700 nm (visible), 700–1000 nm (NIR), 1300–1600 nm (NIR), and 1600–2400 (SWIR). As can be seen by the relative variability scales, going longer in wavelength shows progressively decreasing variability. Figures also include the direct comparison to both the NRLSSI2 and SATIRE-S models; each model has been separately scaled in magnitude to match the TSIS-1 SIM observations over an 81-day averaged period centered on December 7, 2019. For the UV and near UV regions there is overall good agreement with both active region short-term variability and with the long-term SSI trending of the observations with both the models. However, overall better agreement with the observations is found with the NRLSSI2 model for the UV (265–285 nm) region. As shown in the previous section, the SATIRE-S shows excess peak rotational variability relative to the observations (and the NRLSSI2 model). However, apart from the solar rotational variability differences, the irradiance trend of the SATIRE-S UV SSI during the rise of SC25 is in very good agreement with the TSIS-1 observations.

For the near UV (310–400 nm), the TSIS-1 SIM long-term variability increase is less than both model results, with SATIRE-S showing the highest relative variability. This has been discussed previously with respect to the model differences in the 300–400 nm region (Yeo et al., 2015) but has remained an ongoing area of debate, largely due to the limited and more uncertain observations at these longer near UV wavelengths during previous solar cycles. For example, Yeo et al. (2015) note that for the integrated 300–400 nm band the variability amplitude of the descending phase of SC23 is approximately a factor of 2 less than the observations from overlapping instruments – instruments that have been operating for over a decade and near the end of their operational life where relative long-term correction uncertainties are larger (Rottman et al., 2001; Floyd et al., 2003).

In contrast to the near UV variability, in the visible (400–700 nm) the TSIS-1 SIM observations show an irradiance increase in SC25 exceeding both models; the models in this visible range are essentially in mutual agreement. This difference from the SIM observations is most noticeable beginning in late 2021 with a factor of 2 difference over several months (overall difference is ~300 ppm for the last 3 months of 2021). From January 2022 onward, the visible irradiance trend becomes more consistent with both models. For the late 2021 time period of the SIM observations, an abnormally large seasonal temperature effect was experienced by the TSIS-1 instruments due to a high beta angle ISS orbital orientation. For this 3-month duration, larger instrumental correction uncertainties are documented for the TSIS-1 SIM and the SSI observations here cannot be used to validate either of the models.

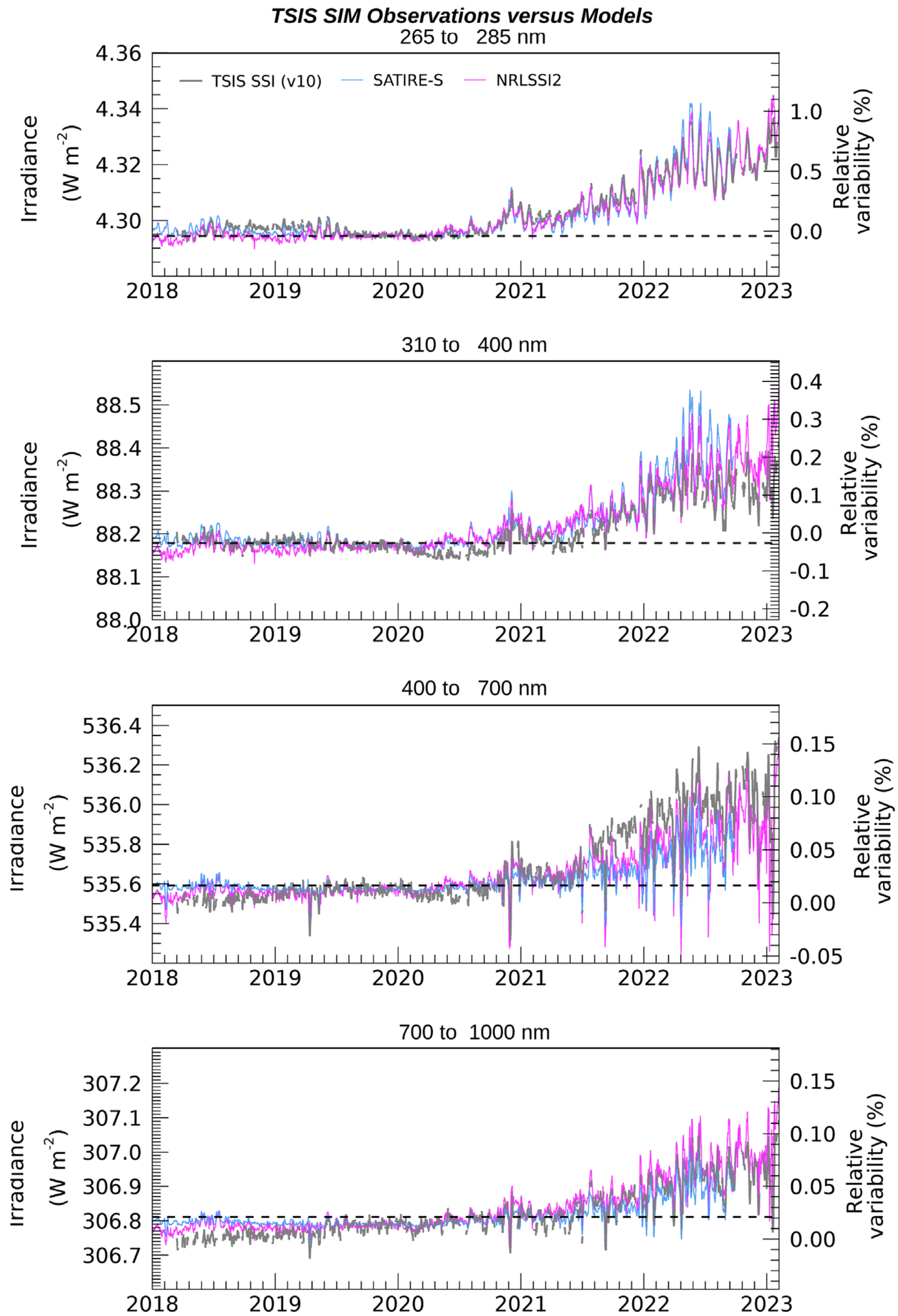

Figure 14. SSI variability comparisons in broadbands covering the UV (265–285 nm & 310–400 nm), Visible (400–700 nm), and near IR (700–1000 nm) of TSIS-1 SIM observations (grey) to the NRLSSI2 model (pink) and SATIRE-S model (blue) over the first 5 years of the TSIS-1 mission.

At the longer wavelengths of 1000–2400 nm shown in Figure 15, the TSIS-1 SIM observations are compared with the models and show that there is generally good irradiance trending agreement with the NRLSSI2 model results (within the instrumental correction uncertainties). However, the SATIRE-S variability in the 1000–1300 nm integrated band shows a smaller irradiance increase (by about half) in the ascending phase of SC25 compared to the observations. In the 1300–1600 nm integrated region, there are further differences between both models in terms of the amplitude and the overall phase of the irradiance changes. Here the TSIS-1 SIM observations and the NRLSSI2 model are more consistent showing a weak increase in irradiance that is in phase with the TSI whereas the SATIRE-S model result shows an overall decrease in irradiance with increasing TSI. Both models capture the sunspot and facular contrast amplitudes consistent with the observations. The TSIS-1 SIM observations for this spectral band (1300–1600 nm) have long-term stability correction uncertainties <50 ppm/year and therefore, by 2023, span an uncertainty range of ±0.03% (1σ). This instrumental

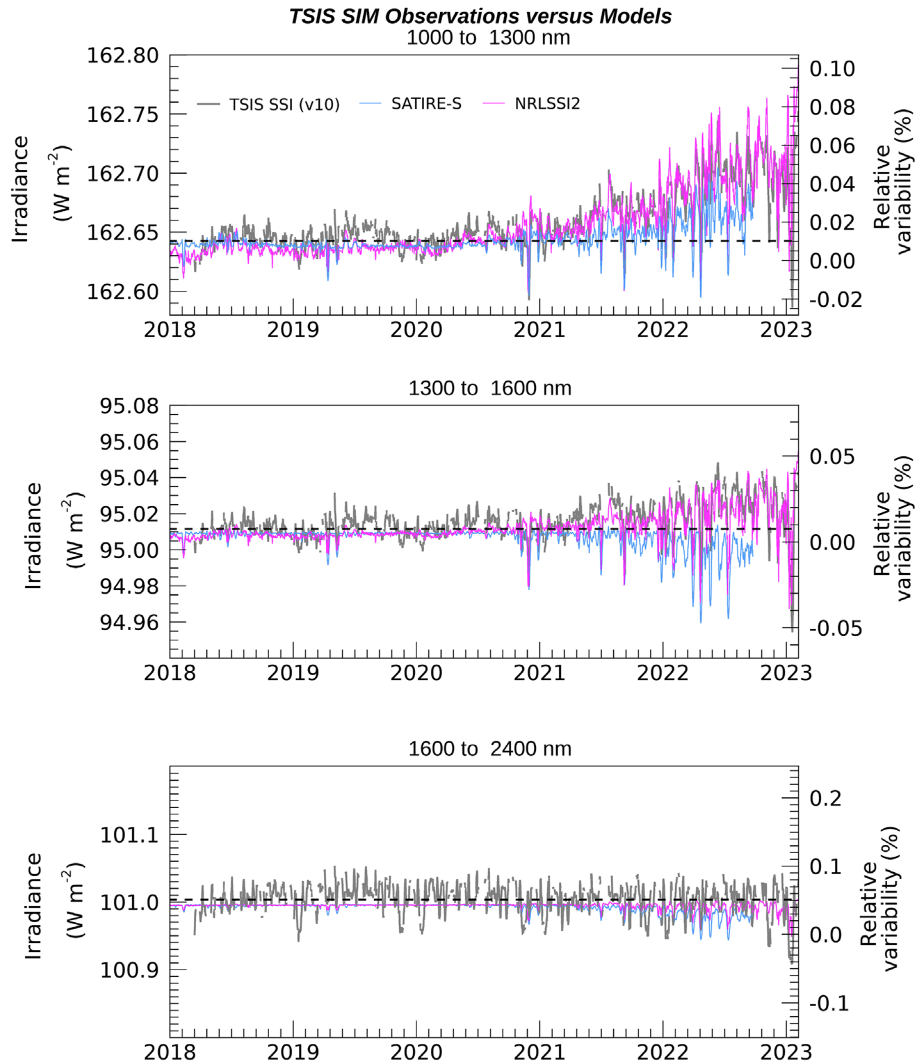

Figure 15. SSI variability comparisons in broadbands covering the near IR (1000–1300 nm & 1300–1600 nm) and short-wave IR (1600–2400 nm) of TSIS-1 SIM observations (grey) to the NRLSSI2 model (pink) and SATIRE-S model (blue) over the first 5 years of the TSIS-1 mission. For the near IR wavelengths there is a small (~100 ppm peak) annual residual signal that is instrumental in origin (see text). This is most noticeable in the first three years of the mission but is also persistent in the SC25 onset. For the longest wavelength region (1600–2400 nm) the measurements here are made by the ESR detector (bolometer-based) and are more sensitive to seasonal adverse temperature time periods due to the ISS orbit in December and January (this is observed as uncorrected irradiance dips at these months for each year).

uncertainty is within the irradiance agreement of NRLSSI2, but outside the irradiance result for SATIRE-S at this point in SC25. We note that this spectral region is near the H-minus solar opacity minimum and has been an active area of SSI variability investigations with predictions of weak but out-of-phase solar cycle behavior (Unruh et al., 1999). Further continuous measurements (past the upcoming SC25 maximum) may be needed to fully quantify the variability for this unique solar irradiance region. Finally, for the longest (SWIR) integrated band (1600–2400 nm) both models are within the larger uncertainties of the TSIS-1 SIM observations where the overall instrument performance can only provide a limit to the SSI variability and bound it within only ~ ±0.05%.

Noticeable in all the IR observations for these bands is a small, but persistent annual correction residual at ~200 ppm peak amplitude levels correlating with the Earth-Sun distance change (1 AU effect). This is most obvious in the early, less active (solar minimum) time period; however, it is likely persistent for the entire 5-year time series but is in the background of the ascending phase amplitudes. This is an instrumental effect and ongoing efforts are focusing on correcting this residual error. The effect is believed to be due to a combination of an annual orbital temperature correction uncertainty as well as a slight time-dependent optical diffraction correction uncertainty. This diffraction change is caused by a solar optical image size change at the prism baffle and modulates the IR throughput dependent on Sun-ISS distance. This is a time-dependent correction in the full parametrization of the SIM measurement equation (Richard et al., 2020). However, this residual error does not factor into the overall stability corrections since the optical degradation corrections are tied to the SIM channel C observations and these only occur every 6 months in early April and early October when the Sun-Earth distance is exactly at the same distance (the unity AU point) for all the inter-channel calibrations. The interpolation of these corrections to the more frequent SIM A (and SIM B) measurements does not provide a constraint against the largest Sun-Earth distance differences (early January at 0.983 AU compared to early July at 1.017 AU) where corrections to the SSI measurement are most sensitive to annual residual errors.

Here we have shown that the TSIS-1 SIM SSI measurements are providing an opportunity to compare to solar variability models that have never been validated on timescales longer than ~3–6 months at wavelengths longer than 400 nm, particularly at IR wavelengths longer than 900 nm. Testing the limits of quantitative assessments of long-term wavelength SSI variability in the visible and near IR in relation to the rotationally modulated variability proxy relationships remains an active and somewhat controversial subject (Harder et al., 2009; Marchenko et al., 2016). To this end, the ongoing, long-term SSI measurements of TSIS-1 SIM will continue to be vital to the overall validation and improvement of the SSI variability models in efforts to eventually elucidate the wavelength dependence of solar-cycle changes and the relationships involving the longer time-scale influence of dark sunspots and bright faculae (and potentially active network) contributions.

5 Conclusions

The TSIS-1 SIM SSI measurements cover a time period that includes the last activity features of solar cycle 24 and the early ascending phase of the onset of solar cycle 25 with a solar minimum during late 2019. The SSI spectrum is found to have significant decreases by as much as 6% in IR irradiance (900–2400 nm) in comparison to several previous SSI reference spectra but in better agreement in the visible and IR irradiance with more recent reference spectra reanalysis efforts.

The TSIS-1 SIM SSI observations during the first five years of operations have demonstrated improved long-term spectral stability with lower trend uncertainties than the SORCE SIM measurements during its early mission operations. Moreover, the spectrally integrated SSI variability is highly consistent with the directly measured TSI variability with a long-term standard deviation of ~50 ppm difference over the first 5 years of continuous operations. All wavelengths in the visible and IR range are shown to be in phase with TSI variability within the measurement stability uncertainties, unlike previous SORCE SIM results during the declining phase of SC23. Specifically, the TSIS-1 SSI to TSI visible and near IR variability correlation plots (ΔTSI/ΔSSI) are nearly linear over the recent rise of SC25 showing an SSI variability near 470 nm ~70% greater than that of the TSI variability whereas in the near IR at 1035 nm the SSI variability is ~30% less than the TSI variability.

We have shown here more consistent results of the SSI measurements at this phase of the TSIS-1 mission. We have also presented initial comparisons of these new SSI observations to SSI model outcomes for the purpose of example during the onset of the current solar activity cycle. Both short-term (solar rotation) and longer-term (ascending phase of SC25) solar variability comparisons to the models show overall good agreement with noted spectral differences in both short-term UV active region contrasts and long-term infrared solar cycle irradiance increases.

Future investigations will provide more in-depth comparisons between measurements and models. For example, over the next several years, as SC25 activity approaches solar maximum conditions, the extant and future SSI observations should provide the opportunity to begin to potentially validate the long-term SSI variability and improve the parameterizations and assumptions utilized by empirical and semi-empirical SSI models. Ultimately, the high-accuracy and high-stability observations of both the TSIS-1 SSI and TSI are critical for future improvements of these solar irradiance variability models and the establishment of a long-term solar irradiance data record.

Acknowledgment

The authors would like to acknowledge funding by NASA (TSIS-1 Mission Operations and Data Processing: Contact #80GSFC18C0056) for initial and ongoing support for the TSIS-1 mission. We are grateful to the many talented LASP engineers and technicians who contributed to the achievement of the new TSIS-1 SIM design, manufacture, calibration, and operations. We also thank the many key contributions of several individuals from the NIST Physical Measurement Laboratory for their efforts in developing and applying innovative laser-based advancements coupled with absolute cryogenic radiometry during the early phases of the calibration activities of the TSIS-1 SIM instrument (specifically, we acknowledge Drs. K. Lykke (Dec.), S. Brown, and J. Rice). We thank the reviewers for providing comprehensive and valuable comments that have improved this manuscript. Finally, we wish to dedicate this paper to Dr. Gary Rottman on the occasion of his 80th birthday in 2024 in recognition of his career of leadership in solar irradiance measurements and their importance in establishing long-term records for Sun-climate research. The editor thanks Mark Weber and an anonymous reviewer for their assistance in evaluating this paper.

Data availability statement

The public data availability for the TSIS-1 mission can be found at the following sites:

SIM L3 data is released on 12-hour and 24-hour cadences:

(a) 12-hour cadence: https://doi.org/10.5067/TSIS/SIM/DATA319
(b) 24-hour cadence: https://doi.org/10.5067/TSIS/SIM/DATA320

TSIS-1 SIM L3 data appears in three locations, in the specified formats:

1) The LASP LISIRD website (ASCII, CSV, and NetCDF)
   12-hour: https://lasp.colorado.edu/lisird/data/tsis_ssi_12hr
   24-hour: https://lasp.colorado.edu/lisird/data/tsis_ssi_24hr
2) The LASP TSIS website (ASCII, IDL SAV file, and NetCDF)
   https://lasp.colorado.edu/home/tsis/data/
3) The NASA DAAC (ASCII)
   https://disc.gsfc.nasa.gov/datasets?page= 1&source=TSIS-1%20SIM

TSIS-1 HSRS CEOS WGCV endorsement: https://calvalportal.ceos.org/tsis-1-hsrs

The public data availability for the TSIS-1 HSRS and FS-HSRS can be found at these links:

(a) TSIS-1 HSRS (202–2730 nm): https://doi.org/10.25980/ta3f-7h90
(b) TSIS-1 FS-HSRS (115–200,000 nm): https://doi.org/10.25980/249q-fs39

References

Ball WT, Rozanov E, Alsing JA, Marsh DR, Tummon F, Mortlock DJ, et al. 2019. The upper stratospheric solar cycle ozone response. *Geophys Res Lett* **46**: 1831–1841. https://doi.org/10.1029/2018GL081501.

Ball WT, Unruh YC, Krivova NA, Solanki S, Harder JW. 2011. Solar irradiance variability: A six-year comparison between SORCE observations and the SATIRE model. *A&A* **530**: A71. https://doi.org/10.1051/0004-6361/201016189.

Bovensmann H, Burrows JP, Buchwitz M, Frerick J, Noel S, et al. 1999. SCIAMACHY: Mission objectives and measurement modes. *J Atmos Sci* **56**: 127–150. https://doi.org/10.1175/1520-0469.

Chapman GA. 1987. Variations of solar irradiance due to magnetic activity. *Ann Rev Astron Astrophys* **25**: 633–667. https://doi.org/10.1146/annurev.aa.25.090187.003221.

Coddington OM, Lean JL, Pilewskie P, Snow M, Lindholm DA. 2016. Solar irradiance climate data record. *Bull Am Meterol Soc* **97**: 1265–1282. https://doi.org/10.1175/BAMS-D-14-00265.1.

Coddington OM, Richard EC, Harber D, Pilewskie P, Woods TN, Chance K. 2021. The TSIS-1 hybrid solar reference spectrum. *Geophys Res Lett* **48**: e2020GL091709. https://doi.org/10.1029/2020GL091709.

Coddington OM, Richard EC, Harber D, Pilewskie P, Woods TN, Snow M, et al. 2023. Version 2 of the TSIS-1 hybrid solar reference spectrum and extension to the full spectrum. *Earth Space Sci* **10**: e2022EA002637. https://doi.org/10.1029/2022EA002637.

Criscuoli S, Marchenko S, DeLand M, Choudhary D, Kopp G. 2023. Understanding Sun-as-a-star variability of solar Balmer lines. *Astrophys J* **951**: 151. https://doi.org/10.3847/1538-4357/acd17d.

Dudok de Wit T. 2022. Detecting undocumented trends in solar irradiance observations. *J Space Weather Space Clim* **12**: 10. https://doi.org/10.1051/swsc/2021041.

Ermolli I, Criscuoli S, Giorgi F. 2011. Recent results from optical synoptic observations of the solar atmosphere with ground-based instruments. *Contrib Astron Obs Skalnaté Pleso* **41**: 73–84. https://api.semanticscholar.org/CorpusID:220827116.

Ermolli I, Matthes K, Dudok de Wit T, Krivova NA, Tourpali K, Weber M, et al. 2013. Recent variability of the solar spectral irradiance and its impact on climate modelling. *Atmos Chem Phys* **13(8)**: 3945–3977. https://doi.org/10.5194/acp-13-3945-2013.

Eyring V, Gillett NP, Achuta Rao KM, Barimalala R, Barreiro Parrillo M, Bellouin N, Cassou C, Durack PJ, Kosaka Y, McGregor S, Min S, Sun Y. 2021. Human influence on the climate system. In: *Climate Change 2021: The Physical Science Basis. Contribution of Working Group I to the Sixth Assessment Report of the Intergovernmental Panel on Climate Change*. Masson-Delmotte V, Zhai P, Pirani A, Connors SL, Péan C, Berger S, Caud N, Chen Y, Goldfarb L, Gomis MI, Huang M, Leitzell K, Lonnoy E, Matthews JBR, Maycock TK, Waterfield T, Yelekçi O, Yu R, Zhou B (Eds.) Cambridge University Press, Cambridge, United Kingdom and New York, NY, USA. pp. 423–552. https://doi.org/10.1017/9781009157896.005.

Fligge M, Solanki SK, Pap JM, Fröhlich C, Wehrli Ch. 2001. Variations of solar spectral irradiance from near UV to the infrared – measurements and results. *J Atmos Sol-Terr Phys* **63**: 1479–1487. https://doi.org/10.1016/S1364-6826(01)00020-7.

Floyd LE, Cook JW, Herring LC, Crane PC. 2003. SUSIM'S 11-year observational record of the solar UV irradiance. *Adv Space Res* **31**: 2111–2120. https://doi.org/10.1016/S0273-1177(03)00148-0.

Fontenla JM, Harder JW, Livingston W, Snow M, Woods T. 2011. High-resolution solar spectral irradiance from extreme ultraviolet to far infrared. *J Geophys Res* **116**: D20108. https://doi.org/10.1029/2011JD016032.

Fontenla JM, White OR, Fox PA, Avrett EH, Kurucz RL. 1999. Calculation of solar irradiances. I. Synthesis of the solar spectrum. *Astrophys J* **518**: 480–499. https://doi.org/10.1086/307258.

Fröhlich C, Romero J, Roth H, Werli C, Andersen BN, et al. 1995. VIRGO: Experiment for helioseismology and solar irradiance monitoring. *Solar Phys* **162**, 101–128. https://doi.org/10.1007/BF00733428.

Gray LJ, Beer J, Geller M, Haigh JD, Lockwood M, et al. 2010. Solar influence on climate. *Rev Geophys* **48(4)**: 1–53. https://doi.org/10.1029/2009RG000282.

Haigh JD. 1996. The impact of solar variability on climate. *Science* **272**: 981–984. https://doi.org/10.1126/science.272.5264.981.

Haigh JD. 2007. The Sun and the Earth's climate. *Living Rev Solar Phys* **4**: 5–59. https://doi.org/10.12942/lrsp-2007-2.

Haigh JD, Winning AR, Toumi R, Harder JW. 2010. An influence of solar spectral variations on radiative forcing of climate. *Nature* **467**: 696–699. https://doi.org/10.1038/nature09426.

Haberreiter M, Schmutz W, Hubeny I. 2008. NLTE model calculations for the solar atmosphere with an iterative treatment of opacity distribution functions. *A&A* **492**: 833–840. https://doi.org/10.1051/0004-6361: 200809503.

Haberreiter M, Schöll M, Dudok de Wit T, Kretzschmar M, Misios S, et al. 2017. A new observational solar irradiance composite. *J Geophys Res Space Phys* **122**: 5910–5930. https://doi.org/10.1002/2016JA023492.

Hansen J, Sato M, Ruedy R, Nazarenko L, Lacis A, et al. 2005. Efficacy of climate forcings. *J Geophys Res* **110**: D18104. https://doi.org/10.1029/2005JD005776.

Harber D, Castleman Z, Drake G, Van Dreser S, Farber N, et al. 2019. Compact total irradiance monitor flight demonstration. In: Vol. **11131** of *Proc SPIE*: *CubeSats and SmallSats for Remote Sensing*, SPIE. p. 111310D. https://doi.org/10.1117/12.2531308.

Harder JW, Fontenla JM, Lawrence G, Woods TN, Rottman GJ. 2005b. The spectral irradiance monitor: Measurement equations and calibration. *Solar Phys* **230**: 169–204. https://doi.org/10.1007/s11207-005-1528-1.

Harder JW, Fontenla JM, Pilewskie P, Richard EC, Woods TN. 2009. Trends in solar spectral irradiance variability in the visible and infrared. *Geophys Res Lett* **36**: L07801. https://doi.org/10.1029/2008GL036797.

Harder JW, Lawrence G, Fontenla J, Rottman G, Woods T. 2005a. The spectral irradiance monitor: Scientific requirements, instrument design, and operation modes. *Solar Phys* **230**: 141–167. https://doi.org/10.1007/s11207-005-5007-5.

Harder JW, Thuillier G, Richard EC, Brown SW, Lykke KR, et al. 2010. The SORCE SIM solar spectrum: Comparison with recent observations. *Solar Phys* **263**: 3–24. https://doi.org/10.1007/s11207-010-9555-y.

Hilbig T, Weber M, Bramstedt K, Noël S, Burrows JP, et al. 2018. The new SCIAMACHY reference solar spectral irradiance and its validation. *Solar Phys* **293**: 121. https://doi.org/10.1007/s11207-018-1339-9.

Hood LL, Misios S, Mitchel DM, Rozanov E, Gray LJ, et al. 2015. Solar signals in CMIP-5 simulations: The ozone response. *Q J Royal Met Soc* **141(692)**: 2670–2689. https://doi.org/10.1002/qj.2553.

IPCC. 2023. Summary for policymakers. In: *Climate Change 2023: Synthesis Report. Contribution of Working Groups I, II and III to the Sixth Assessment Report of the Intergovernmental Panel on Climate Change*. Core Writing Team, Lee H, Romero J (Eds.) IPCC, Geneva, Switzerland. pp. 1–34. https://doi.org/10.59327/IPCC/AR6-9789291691647.001.

Kodera K, Kuroda Y 2002. Dynamical response to the solar cycle. *J Geophys Res* **107(D24)**: 4749. https://doi.org/10.1029/2002JD002224.

Kopp G. 2014. An assessment of the solar irradiance record for climate studies. *J Space Weather Space Clim* **4**: A14. https://doi.org/10.1051/swsc/2014012.

Kopp G. 2021. Science highlights and final updates from 17 years of total solar irradiance measurements from the solar radiation and climate experiment/total irradiance monitor (SORCE/TIM). *Solar Phys* **296**: 133. https://doi.org/10.1007/s11207-021-01853-x.

Kopp G, Lawrence G 2005. The total irradiance monitor (TIM): Instrument design. *Solar Phys* **230**: 91–109. https://doi.org/10.1007/s11207-005-7446-4.

Kren AC, Pilewskie P, Coddington O. 2017. Where does Earth's atmosphere get its energy? *J Space Weather Space Clim* **7**: A10. https://doi.org/10.1051/swsc/2017007.

Krivova NA, Solanki SK, Fligge M, Unruh YC. 2003. Reconstruction of solar irradiance variations in cycle 23: is solar surface magnetism the cause? *A&A* **399**: L1–L4. https://doi.org/10.1051/0004-6361:20030029.

Krivova NA, Solanki SK, Floyd L. 2006. Reconstruction of solar UV irradiance in cycle 23. *A&A* **452**: 631–639. https://doi.org/10.1051/0004-6361:20064809.

Krivova NA, Solanki SK, Unruh YC. 2011. Towards a long-term record of solar total and spectral irradiance. *J Atmos Sol Terr Phys* **73**: 223–234. https://doi.org/10.1016/j.jastp.2009.11.013.

L'Ecuyer TS, Beaudoing HK, Rodell M, Olson W, Lin B, et al. 2015. The observed state of the energy budget in the early twenty-first century. *J Clim* **28**: 8319–8346. https://doi.org/10.1175/JCLI-D-14-00556.1.

Lean JL. 2017. Sun-climate connections. In: *Oxford Research Encyclopedia of Climate Science, id 1*, Oxford University Press. https://doi.org/10.1093/acrefore/9780190228620.013.9.

Lean JL. 2000. Evolution of the Sun's spectral irradiance since the Maunder minimum. *Geophys Res Lett* **27**: 2425–2428. https://doi.org/10.1029/2000GL000043.

Lean JL, DeLand MT. 2012. How does the Sun's spectrum vary? *J Clim* **25**: 2555–2560. https://doi.org/10.1175/JCLI-D-11-00571.1.

Lean JL, Coddington O, Marchenko SV, DeLand MT. 2022. A new model of solar ultraviolet irradiance variability with 0.1–0.5 nm spectral resolution.

Earth Space Sci **9(10)**: e2021EA002211. https://doi.org/10.1029/2021EA002211.

Lean JL, Coddington O, Marchenko SV, Machol J, DeLand MT, Kopp G. 2020. Solar irradiance variability: Modeling the measurements. *Earth Space Sci* **7(8)**: e2019EA000645. https://doi.org/10.1029/2019EA000645.

Lean JL, Cook J, Marquette W, Johannesson A. 1998. Magnetic sources of the solar irradiance cycle. *Astrophys J* **492**: 390–401. https://doi.org/10.1086/305015.

Lean J, Rottman G, Harder J, Kopp G. 2005. SORCE contributions to new understanding of global change and solar variability. *Solar Phys* **230**: 27–53. https://doi.org/10.1007/s11207-005-1527-2.

Lean JL, Rottman GJ, Kyle HL, Woods TN, Hickey JR, Puga LC. 1997. Detection and parameterization of variations in solar mid and near ultraviolet radiation (200 to 400 nm). *J Geophys Res* **102**: 29939–29956. https://doi.org/10.1029/97jd02092.

Marchenko SV, Deland MT, Lean JL. 2016. Solar spectral irradiance variability in cycle 24: Observations and models. *J Space Weather Space Clim* **6**: A40. https://doi.org/10.1051/swsc/2016036.

Matthes K, Funke B, Anderson ME, Barnard L, Beer J, et al. 2017. Solar forcing for CMIP6 (v3.2). *Geosci Model Dev* **10(6)**: 2247–2302. https://doi.org/10.5194/gmd-10-2247-2017.

Matthes K, Kuroda Y, Kodera K, Langematz U. 2006. Transfer of the solar signal from the stratosphere to the troposphere: Northern winter. *J Geophys Res* **111**: D06108. https://doi.org/10.1029/2005JD006283.

Mauceri S, Pilewskie P, Richard E, Coddington O, Harder J, Woods T. 2018. Revision of the Sun's spectral irradiance as measured by SORCE SIM. *Solar Phys* **293**: 161. https://doi.org/10.1007/s11207-018-1379-1.

Mauceri S, Richard E, Pilewskie P, Harber D, Coddinton O, et al. 2020a. Degradation correction of TSIS SIM. *Solar Phys* **295**: 152. https://doi.org/10.1007/s11207-020-01707-y.

Mauceri S, Pilewskie P, Woods T, Béland S, Richard E. 2020b. Intercomparing solar spectral irradiance from SORCE SIM. *Earth Space Sci* **7**: e2019EA001002. https://doi.org/10.1029/2019EA001002.

McClintock WE, Rottman GJ, Woods TN. 2005a. Solar-stellar irradiance comparison experiment II (SOLSTICE II): instrument concept and design. *Solar Phys* **230**: 225–258. https://doi.org/10.1007/s11207-005-7432-x.

McClintock WE, Snow M, Woods TN. 2005b. Solar-stellar irradiance comparison experiment II (SOLSTICE II): Pre-launch and on-orbit calibrations. *Solar Phys* **230**: 259–294. https://doi.org/10.1007/s11207-005-1585-5.

Meehl GA, Arblaster JM, Branstator G, van Loon H. 2008. A coupled air-sea response mechanism to solar forcing in the Pacific region. *J Clim* **21**: 2883–2897. http://www.jstor.org/stable/26259945.

Meehl GA, Washington WM, Wigley TML, Arblaster JM, Dai A. 2003. Solar and greenhouse gas forcing and climate response in the 20th century. *J Clim* **16**: 426–444. https://doi.org/10.1175/1520-0442(2003)016<0426:SAGGFA>2.0.CO;2.

Meftah M, Damé L, Bolsée D, Hauchecorne A, Pereira N, Sluse D, et al. 2018. SOLAR-ISS: A new reference spectrum based on SOLAR/SOLSPEC observations. *A&A* **611**: A1. https://doi.org/10.1051/0004-6361/201731316.

Meftah M, Damé L, Bolsée D, Pereira N, Snow M, et al. 2020. A new version for the SOLAR-ISS spectrum covering the 165–3000 nm spectral region. *Sol Phys* **295**: 14. https://doi.org/10.1007/s11207-019-1571-y.

Preminger DG, Walton SR, Chapman GA. 2002. Photometric quantities for solar irradiance modeling. *J Geophys Res* **107**: 1354. https://doi.org/10.1029/2001JA009169.

Richard E, Harber D, Coddington O, Drake G, Rutkowski J, et al. 2020. SI-traceable spectral irradiance radiometric characterization and absolute calibration of the TSIS-1 spectral irradiance monitor (SIM). *Remote Sens* **12**, 1818. https://doi.org/10.3390/rs12111818.

Richard E, Harber D, Drake G, Rutkowski J, Castleman Z, et al. 2019. Compact spectral irradiance monitor flight demonstration mission. In: Vol. **11131** of *Proc SPIE*: *CubeSats and SmallSats for Remote Sensing*, SPIE. p. 1113105. https://doi.org/10.1117/12.2531268.

Rottman G, Woods T, Snow M, DeToma G. 2001. The solar cycle variation in ultraviolet irradiance. *Adv Space Res* **27**: 1927–1932. https://doi.org/10.1016/S0273-1177(01)00272-1.

Shapiro AI, Schmutz W, Schoell M, Haberreiter M, Rozanov E. 2010. NLTE solar irradiance modeling with the COSI code. *A&A* **517**, A48. https://doi.org/10.1051/0004-6361/200913987.

Shindell DT, Faluvegi G, Schmidt GA. 2020. Influences of solar forcing at ultraviolet and longer wavelengths on climate. *J Geophys Res Atmos* **125 (7)**: e2019JD031640. https://doi.org/10.1029/2019JD031640.

Seppälä A, Matthes K, Randall CE, Mironova IA. 2014. What is the solar influence on climate? Overview of activities during CAWSES-II. *Prog Earth Planet Sci* **1**: 24. https://doi.org/10.1186/s40645-014-0024-3.

Solanki SK, Unruh YC. 1998. A model of the wavelength dependence of solar irradiance variations. *A&A* **329**: 747–753. https://www2.mps.mpg.de/dokumente/publikationen/solanki/j77.pdf.

Solanki SK, Krivova NA, Haigh JD. 2013. Solar irradiance variablity and climate. *Annu Rev Astron Astrophys* **51**: 311–351. https://doi.org/10.1146/annurev-astro-082812-141007.

Stephens G, Freeman A, Richard E, Pilewskie P, Larkin P, Chew C, et al. 2019. The emerging technological revolution in earth observations. *Bull Amer Met Soc* E274–E285. https://doi.org/10.1175/BAMS-D-19-0146.1.

Stephens GL, Li J, Wild M, Clayson CA, Loeb N, et al. 2012. An update on the earth's energy balance in light of new surface energy flux estimates. *Nature Geosci* **5**: 691–696. https://doi.org/10.1038/ngeo1580.

Swartz WH, Stolarski RS, Oman LD, Fleming EL, Jackman CH. 2012. Middle atmosphere response to difference descriptions of the 11-yr solar cycle in spectral irradiance in a chemistry-climate model. *Atmos Chem Phys* **12**: 5937–5948. https://doi.org/10.5194/acp-12-5937-2012.

Tett SFB, Jones GS, Stott PA, Hill DC, Mitchell JFB, et al. 2002. Estimation of natural and anthropogenic contributions to twentieth century temperature change. *J Geophys Res Atmos* **107**: 4306. https://doi.org/10.1029/2000JD000028.

Thuillier G, Bolsée D, Schmidtke G, Foujols T, Nikutowski B, et al. 2014. The solar irradiance spectrum at solar activity minimum between solar cycles 23 and 24. *Solar Phys* **289**: 1931–1958. https://doi.org/10.1007/s11207-013-0461-y.

Thuillier G, Harder JW, Shapiro A, Woods TN, Perrin J-M, et al. 2015. The infrared solar spectrum measured by the SOLSPEC spectrometer onboard the International Space Station. *Solar Phys* **290**: 1581–1600. https://doi.org/10.1007/s11207-015-0704-1.

Thuillier G, Hersé M, Labs D, Foujols T, Peetermans W, et al. 2003. The solar spectral irradiance from 200 to 2400 nm as measured by the SOLSPEC spectrometer from the Atlas and Eureca missions. *Solar Phys* **214**: 1–22. https://doi.org/10.1023/A:1024048429145.

Upton L, Hathaway D. 2023. Solar cycle precursors and the outlook for cycle 25. *J Geophys Res Space Phys* **128**: e2023JA031681. https://doi.org/10.1029/2023JA031681.

Unruh YC, Solanki SK, Fligge M. 1999. The spectral dependence of facular contrast and solar irradiance variations. *A&A* **345**: 635–642. https://www.scopus.com/record/display.uri?eid=2-s2.0-0000172578&origin=inward&txGid=82221695333ac8a552bd58454bcd2f6d.

van Loon H, Meehl GA, Shea DJ. 2007. Coupled air-sea response to solar forcing in the Pacific region during northern winter. *J Geophys Res* **112**: D02108. https://doi.org/10.1029/2006JD007378.

Wang W, Matthes K, Tian W, Park W, Shangguan M, Ding A. 2019. Solar impacts on decadal variability of tropopause temperature and lower stratospheric (LS) water vapour: a mechanism through ocean–atmosphere coupling. *Clim Dynam* **52**: 5585–5604. https://doi.org/10.1007/s00382-018-4464-0.

Weatherhead EC, Harder J, Araujo-Pradere EA, Bodeker G, English JM, et al. 2017. How long do satellites need to overlap? Evaluation of climate data stability from overlapping satellite records. *Atmos Chem Phys* **17**: 15069–15093. https://doi.org/10.5194/acp-17-15069-2017.

Wehrli C, Schmutz W, Shapiro A. 2013. Correlation of spectral solar irradiance with solar activity as measured by VIRGO. *A&A* **556**: L3. https://doi.org/10.1051/0004-6361/201220864.

White MG, Heuerman K, Shaw PS, Stephens MS, Tomlin NA, et al. 2022. Decadal validation of the LASP TRF cryogenic radiometer by NIST, and establishment of a replacement room temperature standard. *Metrologia* **59**: 065006. https://doi.org/10.1088/1681-7575/ac89f5.

Wild M, Folini D, Hakuba MZ, Schär C, Seneviraten SI, et al. 2015. The energy balance over land and oceans: An assessment based on direct observations and CMIP5 climate models. *Clim Dynam* **44**: 3393–3429. https://doi.org/10.1007/s00382-014-2430-z.

Wild M, Folini D, Schär C, Loeb N, Dutton EG, König-Langlo G. 2013. The global energy balance from a surface perspective. *Clim Dynam* **40**: 3107–3134. https://doi.org/10.1007/s00382-012-1569-8.

Wild M, Hakuba MZ, Folini D, Dörig-Ott P, Schär C, et al. 2019. The cloud-free global energy balance and inferred cloud radiative effects: An assessment based on direct observations and climate models. *Clim Dynam* **52**: 4787–4812. https://doi.org/10.1007/s00382-018-4413-y.

Willson RC, Gulkis S, Janssen M, Hudson HS, Chapman GA. 1981. Observations of solar irradiance variability. *Science* **211**: 4483. https://doi.org/10.1126/science.211.4483.700.

Woods TN. 2008. Recent advances in observations and modeling of the solar ultraviolet and X-ray spectral irradiance. *Adv Space Res* **42**: 895–902. https://doi.org/10.1016/j.asr.2007.09.026.

Woods TN, Chamberlin PC, Harder JW, Hock RA, Snow M, et al. 2009. Solar irradiance reference spectra (SIRS) for the 2008 whole heliosphere interval (WHI). *Geophys Res Lett* **36**: L01101. https://doi.org/10.1029/2008GL036373.

Woods TN, Eparvier FG, Harder JH, Snow M. 2018. Decoupling solar variability and instrument trends using the multiple same-irradiance-level (MuSIL) analysis technique. *Solar Phys* **293**: 76. https://doi.org/10.1007/s11207-018-1294-5.

Woods TN, Snow M, Harder J, Chapman G, Cookson A. 2015. A different view of solar spectral irradiance variations: Modeling total energy of six-month intervals. *Solar Phys* **290**: 2649. https://doi.org/10.1007/s11207-015-0766-0.

Yeo KL, Ball WT, Krivova NA, Solanki SK, Unruh YC, Morrill J. 2015. UV solar irradiance in observations and the NRLSSI and SATIRE-S models. *J Geophys Res* **120**: 6055–6070. https://doi.org/10.1002/2015JA021277.

Yeo KL, Krivova NA, Solanki SK, Glassmeier KH. 2014. Reconstruction of total and spectral solar irradiance from 1974 to 2013 based on KPVT, SoHO/MDI, and SDO/HMI observations. *A&A* **570**: A85. https://doi.org/10.1051/0004-6361/201423628.

Appendix A

TSIS-1 SIM spectral degradation corrections and stability analysis

The lessons learned from the design and nearly two decades of continuous solar viewing operations of the SORCE SIM instrument provided the guidance for the improvements in accuracy and long-term spectral stability for the TSIS-1 SIM instrument. These instrument improvements and calibration advancements have been discussed in detail previously (Richard et al., 2020). A major change to reduce the uncertainties of the long-term stability corrections was the addition of a third, redundant spectral channel to further correct the solar exposure degradation.

The three TSIS-1 SIM channels are duty-cycled with respect to solar exposure to track and correct optical degradation due to the solar exposure in the primary solar-observing channel. The relative inter-channel exposure rates have been nearly constant throughout the TSIS-1 mission. Duty-cycling rates and observation times for SIM are shown in Table A1. The duty-cycle ratio between SIM Channel B and SIM Channel A is 11.8%, and the ratio between SIM Channel C and SIM Channel B is 11.1%.

The initial SIM spectral degradation corrections using three redundant channels with different duty cycles has been previously discussed (Mauceri et al., 2020a). Both the spectral and temporal degradation are tracked and corrected through common solar measurements by all three SIM channels operating under very different cumulative solar exposure times. The instrument operation plan for the entire TSIS-1 mission over

Table A1. TSIS-1 SIM exposure rates.

SIM channel	Spectrum cadence	Cumulative observing time (days)*
Channel A, Primary	Twice daily	192.4
Channel B, Secondary	~Once per week	22.6
Channel C, Tertiary	Once every 6 months	2.5

* Cumulative solar exposure through January 2023.

the last 5 years has been based on maintaining a constant exposure ratio of SIM Channel B to SIM Channel A at ~12%. Using the SIM Channel A, the twice daily SSI from 200 nm to 2400 nm is recorded by a series of photodiode detectors covering the UV to near IR range (200–1650 nm) and the ESR for the infrared wavelengths from 1650 to 2400 nm to produce a 12-hour and 24-hour SSI data product.

Figure A.1 presents the measured SSI data for several example wavelengths spanning the UV to the near IR for all three SIM channels over the current TSIS-1 mission through January 2023. The time series data here includes the degradation uncorrected channel irradiance for all three channels and the final corrected channel A irradiance. The largest spectral degradation occurs at ~220 nm which shows a decrease in signal throughput of ~10% for 5 full years of continuous operations. As of January 2023, the TSIS-1 SIM Channel A exposure of 192 days is approximately 7 times smaller than SORCE SIM degradation at the same point – a direct consequence of the contamination mitigation efforts in both the design and assembly of the TSIS-1 SIM over the SORCE SIM. Another key advantage of TSIS-1 SIM is that a third, redundant spectral channel was implemented and limited to having only two observations per year.

As can be seen from Figure A.1, the degradation occurs together with increasing solar activity, therefore requiring the common measurements from the different channels to separate the instrumental degradation from the true solar variability. The ratios of the different SIM channels are parameterized based on the actual cumulative solar exposure time for each channel and not the calendar time. By taking the ratios of the individual channel measurements made on the same calendar time (i.e., same Sun) we are able to separate the optical degradation trend from the solar activity. The current rate of degradation is stable and the measurement signal-to-noise ratios (SNRs) remain high thus the ability to fit these ratios to empirical degradation functions improves the overall efficiency of the stability corrections as nominal operations continue. As can be seen in Figure A.1, increasing solar activity from SC25 is evident in the decay curves as a function of calendar date. The method to quantify the spectral degradation rates for TSIS-1 SIM is outlined below.

With reference to Figure A.1, the measured, uncorrected spectral irradiance as a function of wavelength and mission time is denoted $\mathcal{E}_i(\lambda, t)$, where i is the channel reference (A, B, or C). The corrected (true) spectral irradiance is denoted $E_i(\lambda, t)$, again for the ith channel. The process for generating the corrected SSI from the direct measurements (uncorrected) SSI involves using multiple SIM channels together. The immutable agreement of the corrected SSI, measured at the same time (i.e., same Sun) means that for each channel A and channel B irradiance at a given wavelength and a given calendar time, the following condition must hold

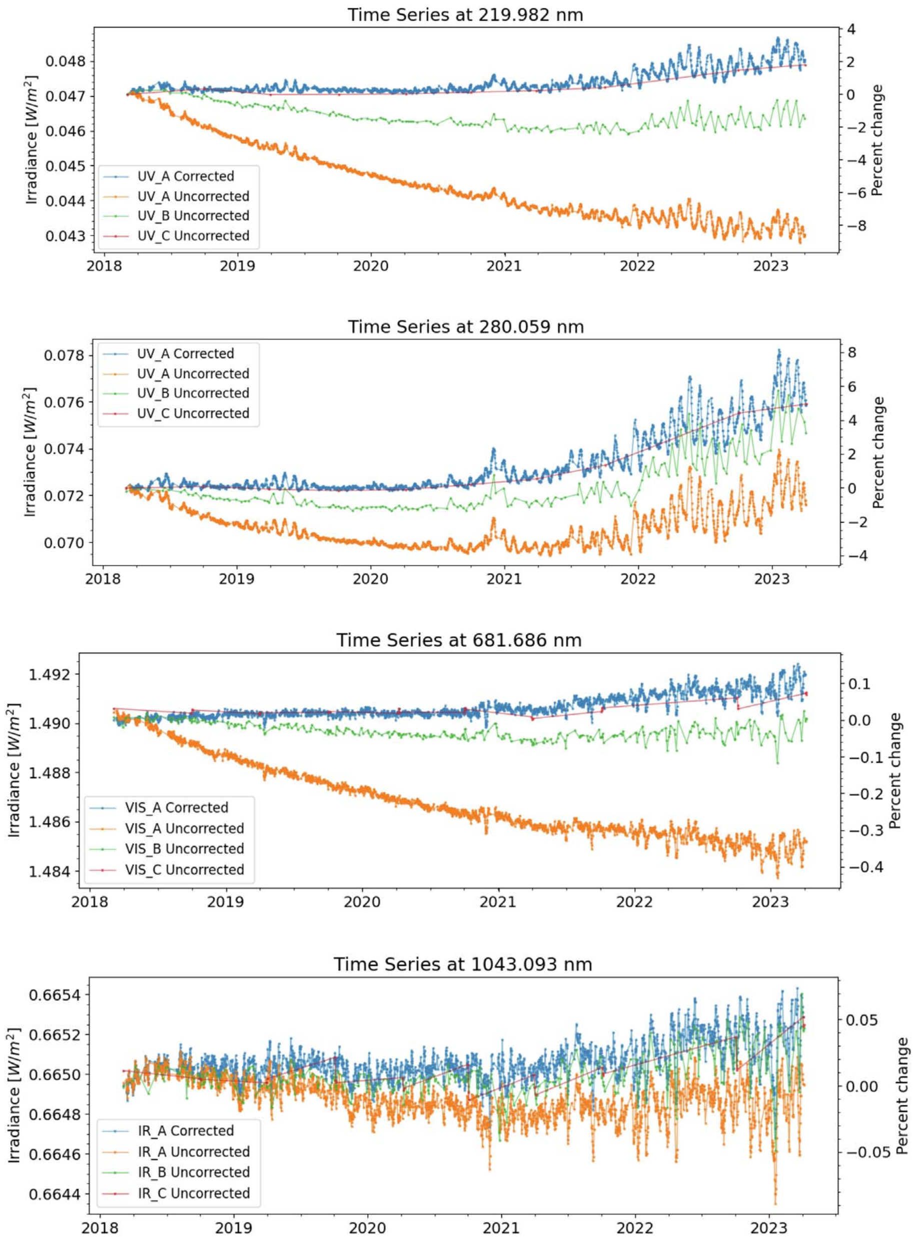

Figure A.1. Examples of SIM channel data as a function of mission calendar day for UV through near-IR wavelengths. The orange, green, and red traces show the raw, uncorrected SSI data for SIM Channel A, B, and C, respectively. Note the relative percent change scale on the right axis. The dominant optical degradation occurs in the UV at 220 nm where the optical throughput has decreased by ~10% over 5 years for SIM Channel A. Degradations for SIM Channel B and C are less in direct proportion to the decreases in solar exposure time for those channels. The Channel C data are used to correct Channel B data, and then the corrected Channel B data are used to correct Channel A data (blue traces in the plots). As can be seen in the visible (682 nm) and near-IR (1043 nm) plots, optical degradation is relatively small but still requires correction. Channel-to-channel ratio fits versus solar exposure time separates the degradation from solar activity changes.

$$E'_A(\lambda, t') = E'_B(\lambda, t') \tag{A.1}$$

where E' denotes the true (corrected) spectral irradiance, t' is a specific calendar time. Likewise, for the less frequent channel B and channel C common measurements at the same calendar time, t, we have

$$E'_B(\lambda, t) = E'_C(\lambda, t). \tag{A.2}$$

To generate the corrected SSI from the measured (uncorrected) SSI we apply a spectral degradation function that is parameterized based not only on calendar time but also on the cumulative solar exposure time for a given channel. Therefore, as an example for SIM channel C, we have

$$E'_C(\lambda, t') = \frac{\mathcal{E}_c(\lambda, t')}{D\left(\lambda, t', t_e^C\right)} \tag{A.3}$$

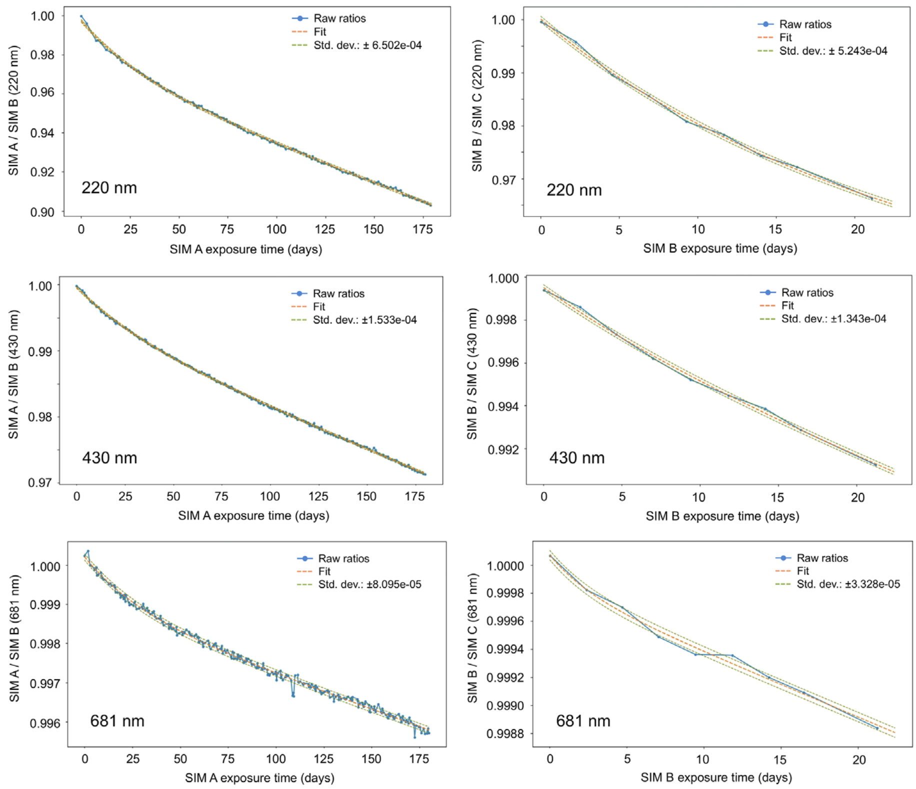

Figure A.2. Examples of the channel-to-channel ratios between SIM channels (recorded on the same calendar days) as a function of solar exposure time. Because the different channels are measured nearly simultaneously, the spectral ratios are free of solar activity and reflect the optical throughput degradation due to solar exposure. The degradation is fit with a two-term exponential decay as a function of the cumulative solar exposure time. The SIM B irradiance used in the SIM A/SIM B ratio is the corrected SIM B irradiance determined from the SIM B/SIM C ratio fits. These ratios are generated for each wavelength across the spectrum so degradation fits provide a spectrally dependent decay constant for use in data processing. The standard deviations of the fits are used to derive the spectrally dependent correction rate uncertainties (ppm/yr) over the current mission. As of January 2023, these plots show that for 220 nm the degradation is 10% for SIM A and 3% for SIM B, at 430 nm 3% for A and 0.8% for B, and at 681 nm 0.4% for A and ~0.1% for B.

where $\mathcal{E}_c(\lambda, t')$, is the SIM C measured, uncorrected spectral irradiance, and again t' is a specific calendar time and t_e is the specific cumulative exposure time for a given channel (here for the SIM C channel). This exposure time is accurately monitored for each SIM channel and is the cumulative time solar flux is impinging on the prism when the entrance shutter is open. Based on a uniform exposure profile as a function of time, we assume an exponential decay for the measured SSI as a function of exposure time with a decay constant κ, such that

$$D\left(\lambda, t', t_e^C\right) \propto e^{-\kappa(\lambda, t')\cdot t_e^C}. \tag{A.4}$$

To derive the spectral decay constant as a function of wavelength, κ, we use direct spectral ratios of the measured SSI at common calendar times (i.e., the same Sun)

$$\frac{\mathcal{E}_B(\lambda, t')}{\mathcal{E}_C(\lambda, t')} = e^{-\kappa(\lambda, t')\left[t_e^B - t_e^C\right]}. \tag{A.5}$$

A similar relationship applies to the more frequent SIM A and SIM B channel ratios, but with a different, unique decay constant. For the TSIS-1 SIM instrument, the common channel A and B ratios covering the full wavelength range occur approximately weekly with the cumulative solar exposure of channel B remaining at 11.8% that of channel A. The common channel B and C ratios occur once every 6 months at equal 1 AU points in early April and early October every year. These specific calendar times are chosen to maintain a spatially uniform degradation image on the SIM C prism due to the changes in the optical image size with the 3.34% annual changes in Sun-to-Earth (ISS) distance. This timing also maintains a uniform decay rate with exposure time and avoids the ~6.7% 6-month maximum difference in solar flux with distance between January and July. Note that there are no spectral cut-off filters prior to the prism, therefore all wavelengths of solar radiation impinge on the prism. Solar radiation at wavelengths <200 nm is the dominant optical degradation flux due to cumulative exposure.

To ultimately correct the degradation of the SIM Channel A measured irradiances, common spectral and temporal scans are recorded between SIM Channel A and SIM Channel B once per day using both the photodiodes and the ESR over common wavelength intervals of the spectrum. To limit the SIM Channel B solar exposure, this comparison is done on one orbit for SIM Channel B exposure and therefore needs 19 days of ESR scans to cover the full wavelength range of the SSI spectrum (SIM full photodiode scans covering 200–1650 nm on SIM B occur every

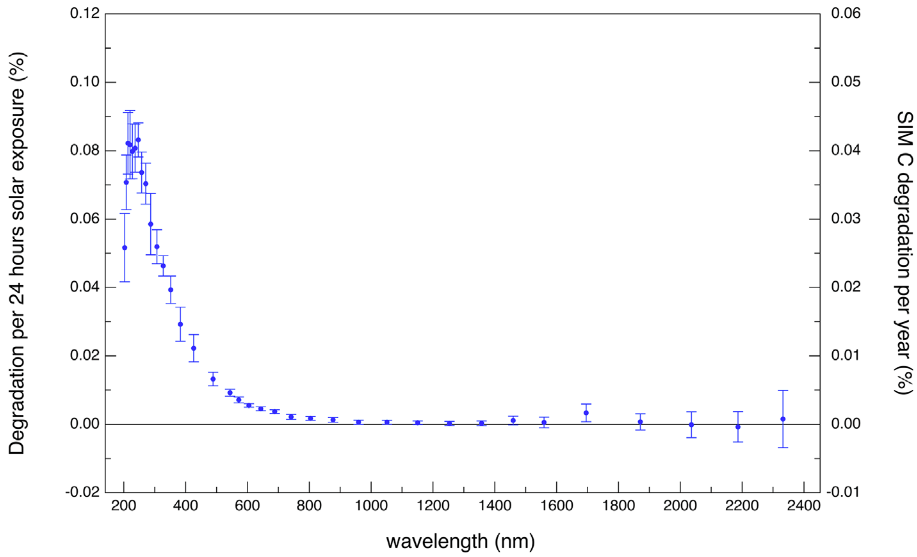

Figure A.3. TSIS-1 SIM spectral degradation rate as a function of solar exposure. Results here are derived from the SIM A to SIM B spectral ratios (as defined by the form of Eq. (A.5)) and the exponential fits. The individual $1-\sigma$ error bars are representative of the standard deviation of the exponential fits to the cumulative solar exposure time. The dominant degradation occurs near 220 nm and is plotted as a rate based on 24-hours of solar exposure. The SIM channel C is corrected with this degradation rate based on the SIM channel C cumulative exposure time. SIM Channel C experiences 12 h of solar exposure per year (6 h per 6-month calibration cadence).

8 days and are calibrated by the common ESR scans). However, the coincident, common spectral scans between SIM Channel A and SIM Channel B cover the same wavelength region at the same time and thus remove any solar variability in the ratios to determine the degradation factors. This exposure schedule has remained constant throughout the entire TSIS-1 mission. To correct the degradation in the SIM Channel B, the least exposed SIM Channel C is used. Every 6 months at the unity AU Earth-Sun distance (early April and early October) coincident spectral scans over common wavelength regions are done between Channel C and Channel B. Solar exposure-related spectral degradation corrections are generated based on this approach across the full measured spectrum (200–2400 nm). Fits to the exponential decay functions of the Channel B to Channel C ratios generate a corrected SIM Channel B irradiance that is then used to correct the SIM Channel A (twice daily) measurements. Figure A.2 shows several examples of this from the UV to visible wavelengths (220 nm, 430 nm, and 681 nm). The left column plots are the SIM Channel A to SIM Channel B ratios plotted as a function of SIM A solar exposure. The right column plots are the corresponding SIM Channel B to SIM Channel C ratios as a function of SIM B solar exposure.

Per the methodology discussed above, exponential fits (as a function of exposure time) are generated for these common spectral ratios to yield a degradation rate and rate uncertainty. Based on the SIM A to SIM B spectral ratios, we derive a wavelength-dependent degradation correction function that is parameterized by solar exposure time. Figure A.3 shows the derived spectral degradation rate per 24 h of solar exposure. This is applied to correct the least exposed channel C data to generate a corrected SSI spectrum every 6 months. Notice here that the degradation rate is a smooth function of wavelength, peaking near 220 nm and then decreasing to near zero by 900 nm and at the noise limit of detection. Recall that SIM Channel C is

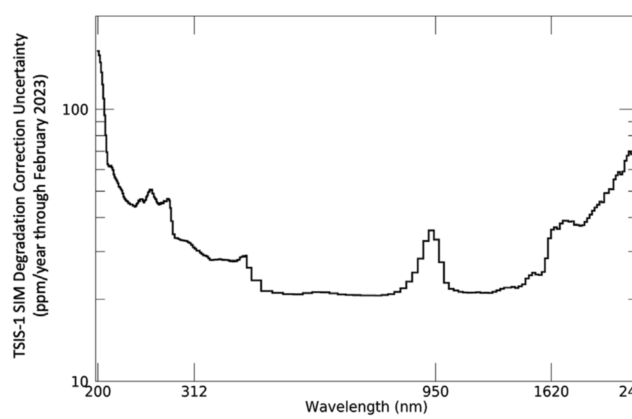

Figure A.4. TSIS-1 SIM degradation correction uncertainties for the spectral stability corrections (relative ppm/year) as a function of wavelength for the binned sampling of the Level-3 SSI data product through February 2023. The spectral sampling involves 1 nm bins for 200–280 nm, 2.5 nm bins for 281–400 nm, and then 22.5 nm bins for wavelengths greater than 400 nm. Detector (and gain) transition regions are apparent in the relative uncertainty by the strongly changing gradients across the spectra, noticeable in the 800–1000 nm region (visible to IR detector transition) and at ~1650 nm (ESR detector transition). The numeric wavelength labels designate the various detector transitions across the spectrum in producing the final SSI data product.

exposed only in early April and October and each calibration scan accumulates 6 h of solar exposure, resulting in 12 h of exposure per year. The corrected SIM channel C SSI is then used to correct the SIM B SSI which then corrects the daily SIM A SSI based on the cumulative solar exposure for each channel (cf. Fig. A.1). This is completed for all wavelengths across the full spectrum to generate the stability corrections and uncertainties *per annum* for the mission.

The SIM solar irradiance stability correction uncertainties based on the first five years of the mission are presented in Figure A.4. Here the degradation analysis has been completed for all wavelengths and applied to the SIM SSI final data product. Shown in the figure is the relative uncertainty in the spectral degradation rate (in ppm/year) after five years of continuous operations. Since the degradation function as seen in Figure A.3 varies smoothly with wavelength across the measured spectrum, we make use of spectral binning to decrease the uncertainties in the application of the corrections. Based on the gradients with wavelength – relatively large in the UV and decreasing to flat for the longer wavelengths – we use spectral bin widths of 1 nm from 200 to 280 nm, 2.5 nm from 281 to 400 nm, and 22.5 nm for wavelengths longer than 400 nm.

Cite this article as: Richard E, Coddington O, Harber D, Chambliss M, Penton S, et al. 2024. Advancements in solar spectral irradiance measurements by the TSIS-1 spectral irradiance monitor and its role for long-term data continuity. *J. Space Weather Space Clim.* **14**, 10. https://doi.org/10.1051/swsc/2024008.